

Elasticity sampling links thermodynamics to metabolic control

Wolfram Liebermeister

Charité - Universitätsmedizin Berlin, Institut für Biochemie
Charitéplatz 1, 10117 Berlin // wolfram.liebermeister@gmail.com

Abstract

Metabolic networks can be turned into kinetic models in a predefined steady state by sampling the reaction elasticities in this state. Elasticities for many reversible rate laws can be computed from the reaction Gibbs free energies, which are determined by the state, and from physically unconstrained saturation values. Starting from a network structure with allosteric regulation and consistent metabolic fluxes and concentrations, one can sample the elasticities, compute the control coefficients, and reconstruct a kinetic model with consistent reversible rate laws. Some of the model variables are manually chosen, fitted to data, or optimised, while the others are computed from them. The resulting model ensemble allows for probabilistic predictions, for instance, about possible dynamic behaviour. By adding more data or tighter constraints, the predictions can be made more precise. Model variants differing in network structure, flux distributions, thermodynamic forces, regulation, or rate laws can be realised by different model ensembles and compared by significance tests. The thermodynamic forces have specific effects on flux control, on the synergisms between enzymes, and on the emergence and propagation of metabolite fluctuations. Large kinetic models could help to simulate global metabolic dynamics and to predict the effects of enzyme inhibition, differential expression, genetic modifications, and their combinations on metabolic fluxes. MATLAB code for elasticity sampling is freely available.

Abbreviations: MCA: Metabolic control analysis; FBA: Flux balance analysis; MoMA: Minimization of metabolic adjustment; ORACLE: Optimization and risk analysis of complex living entities; SKM: Structural kinetic modelling

1 Introduction

How will changes in nutrient supply, enzyme-inhibiting drugs, or genetic modifications affect the metabolic fluxes in cells? Will there be long-range effects, or are local perturbation compensated by changes of the surrounding metabolite levels [1]? Mechanistically, metabolic fluxes are shaped by metabolic network structure, reaction thermodynamics, enzymatic rate laws, allosteric regulation, and regulation of enzyme levels. Large-scale flux, metabolite, and protein data [2] provide a comprehensive picture of metabolism, but turning this knowledge into simulations is difficult. Metabolic networks, comprising thousands of reactions, have been generated from genome sequences [3, 4]. Stoichiometric models can be used to sample possible fluxes [5], and thermodynamic analyses [6, 7, 8, 9] can link them to metabolite levels and equilibrium constants via the reaction Gibbs free energies. Flux analysis methods like FBA [10, 11], MoMA [12], ROOM [13], or flux minimisation [14] can predict favourable flux distributions according to heuristic assumptions [15], but to model how metabolic fluxes are controlled mechanistically, the enzymatic rate laws and their allosteric regulations need to be known. Kinetic models can be used to simulate local perturbations like differential expression of enzymes, varying supply and demand, enzyme inhibition by drugs, or genetic modifications, and to predict the perturbed steady states.

Metabolic fluxes depend on enzyme activities (and therefore, on enzyme levels, inhibitors, or enzyme isoforms), on metabolic supply and demand, and on the growth rate. The effects of these factors on the global fluxes is complicated: if the metabolite levels were fixed, each reaction flux would rise proportionally with the enzyme level. However, since metabolite levels also respond to perturbations, how will stationary fluxes be affected, eventually, by differential expression? Stoichiometric models alone cannot answer this question because the system responses depends on the rate laws, enzyme saturation, and allosteric regulation. In kinetic models, external metabolite levels, enzyme levels, or parameters like temperature or the dilution rate affect the steady state levels and fluxes, and the effects of changing parameters can be approximated by response coefficients. They describe, for each single enzyme level (or other parameter), how a small perturbation would affect the output variables in steady state.

Attempts to turn metabolic networks into kinetic models and to integrate kinetic, thermodynamic, and metabolic data have to address a number of issues: (i) finding realistic rate laws and rate constants; (ii) guaranteeing a consistent equilibrium state with metabolite levels that make all fluxes vanish; (iii) guaranteeing, and possibly predefining, a reference state with realistic fluxes and metabolite levels; and (iv) allow for variability and uncertainties both in rate constants and in the metabolic state. A number of standard rate laws – such as mass-action, power-law [16], linlog [17], or modular rate laws [18, 19] – have been proposed, and the usage of reversible rate laws, together with rate constants satisfying Wegscheider conditions and Haldane relations, can guarantee a consistent equilibrium state. Given a kinetic model and the levels of enzymes and external metabolites, one can determine a steady state numerically. However, to pinpoint a biochemically plausible state, it is practical to predefine stationary fluxes and to determine rate laws and metabolite levels that match these fluxes. There are several options: given feasible fluxes, reversible rate laws, and feasible rate constants, one may determine consistent metabolite levels and solve for the enzyme levels [20, 21, 22], or one may optimise the metabolite concentrations under thermodynamic constraints for a minimal enzyme cost [23]. In both cases, thermodynamic correctness is guaranteed.

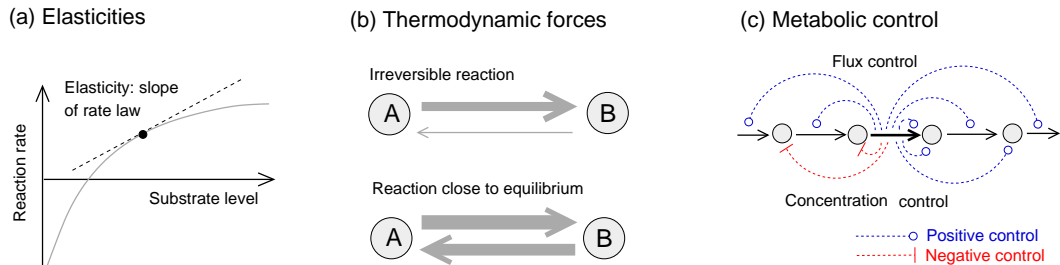


Figure 1: **Elasticities, thermodynamic forces, and metabolic control.** (a) Reaction rates depend on metabolite levels (substrate level shown on x-axis), and their derivatives are called reaction elasticities. (b) In irreversible reactions (with driving forces $A = RT \ln \frac{v^+}{v^-}$ close to infinity), the forward flux dominates and the product elasticity almost vanishes; in reactions close to equilibrium (driving force $A \approx 0$), the net flux results from a small difference of large forward and reverse fluxes, and the scaled elasticities $E_{c_i}^{v_l} = \frac{c_i}{v_l} \frac{\partial v_l}{\partial c_i}$ diverge. (c) Control coefficients describe how perturbed reactions would affect the fluxes or metabolite levels in steady state. They reflect the network structure and flux distribution (for instance, metabolites will accumulate in front of a blocked enzyme and be depleted behind it), but the quantitative values depend on the elasticities. For instance, a strongly driven reaction, with its very low product elasticity, would deprive all downstream enzymes of their flux control.

When a model is built, rate constants may be uncertain or unknown, especially for less well-studied organisms, and enzyme or metabolite levels may vary between experiments. To account for variability and uncertainties, one may use model ensembles in which some features, like network structure and flux distribution, are fixed, while others, like the metabolite levels, are sampled from random distributions [24, 25]. Any model construction method in which variables are freely chosen, without violating any constraints, can be turned into a method for model sampling. From a number of sampled models, we can estimate the distributions in the ideal, infinitely large ensemble, compute the probabilities for certain types of behaviour, and see how they depend on factors like network structure, reference fluxes, and rate laws. Properties that are common to many model instances can be attributed to the model structure. One may also compare structural variants of a model and search for systematic differences that stand out from the random variation.

The ORACLE framework [26, 27, 28, 29] and Structural Kinetic Modelling (SKM, [30, 31]) construct metabolic models by sampling the reaction elasticities for a predefined reference state. The scaled elasticities $E_{c_i}^{v_l} = \frac{c_i}{v_l} \frac{\partial r_l}{\partial c_i}$ are the direct sensitivities of reaction rates $r_l(\mathbf{c})$ to the reactant levels c_i , at the reference point where $r_l(\mathbf{c}) = v_l$. Many dynamic analyses do not require a full kinetic model, but a linearised version that approximates the dynamics around a reference state, based on network structure and elasticities. Such models can describe the dynamics of small fluctuations, caused by static or periodic parameter perturbations or by chemical noise. There exists powerful theory for optimal control and model reduction of linear models [32], and the elasticities are also the basis of metabolic control analysis (MCA, see Figure 1). Metabolic Control Analysis (MCA) [33, 34] traces local perturbations of reaction rates and predicts their long-term effects on the global steady state. The response of steady-state fluxes and concentrations to local perturbations is described by two types of sensitivities, the response and control coefficients, which follow from the reaction elasticities (see appendix I.2). The effects of enzyme inhibition, optimal

enzyme usage [35], and parameter uncertainty or variability [24] can be predicted from a Taylor-expansion of steady states, based on the response coefficients. Second-order response coefficients [36] describe synergies between enzyme pairs and play a role in predicting optimal differential expression [37]; spectral response coefficients describe fluctuations of fluxes and metabolite levels in systems with periodic [38, 39] or stochastic [24] parameter fluctuations.

ORACLE and SKM relate the scaled elasticities in a given steady state to saturation values, which are treated as free variables and sampled from random distributions. As a constraint, the sparsity structure of the elasticity matrix, as determined from the network structure and allosteric regulation arrows, is used. Since reaction rates increase with substrate levels and decreases with product levels, the elasticities' signs are predetermined by the flux directions, and possible ranges can be derived from the rate laws (e.g., $]0, 1[$ for the substrate in a mass-action rate law). Each sampled elasticity matrix yields a linearised kinetic model, whose Jacobian matrix determines the dynamic behaviour close to the reference state and, in particular, its stability. By sampling many elasticity matrices for a network, one can explore its possible types of dynamics and assess their probabilities. By selecting kinetic models with specific features – e.g., stable oscillations – and analysing their elasticities, one may spot model details (e.g., inhibition arrows) that affect these features [30]. Each linearised model could be realised by many kinetic models with different rate laws. However, for the dynamics close to the reference state, these differences do not matter.

The existing sampling approaches, however, have a major limitation: independent sampling is only valid for irreversible rate laws. In models with reversible rate laws – which are necessary to guarantee consistent equilibrium states – the forward and reverse fluxes are subject to thermodynamic constraints, which make the elasticities dependent. The reason is as follows. Metabolic states are shaped by reaction Gibbs free energies, which reflect a disequilibrium between substrate and product levels and determine the flux directions. The negative reaction Gibbs free energy (or reaction affinity) $A = -\Delta_r G$ will later be called thermodynamic driving force. Depending on the reactant levels, reactions can vary between two extremes, equilibrium reactions and irreversible reactions. Equilibrium reactions have a zero driving force, and their forward and reverse microscopic fluxes v^+ and v^- cancel out, so the net flux $v = v^+ - v^-$ vanishes. Irreversible reactions have large driving forces and negligible reverse fluxes v^- and their net flux is dominated by the forward flux v^+ . By setting the ratio v^+/v^- , the driving forces partly determine the elasticities: for instance, if a driving force becomes very large, the rate becomes practically independent of the product levels, and the product elasticities vanish. Their dependence on driving forces makes the elasticities dependent as well, potentially across the entire model, and ignoring this fact can lead to inconsistent models [19] (for an example, see appendix C).

2 Results

2.1 Model construction based on elasticity sampling

The reaction elasticities of many reversible rate laws can be computed from the thermodynamic forces and from saturation values, which are not constrained by thermodynamics [19]. The elasticity formula for modular rate laws (Eq. (1) in Methods) allows for a consistent sampling of elasticities and paves the way

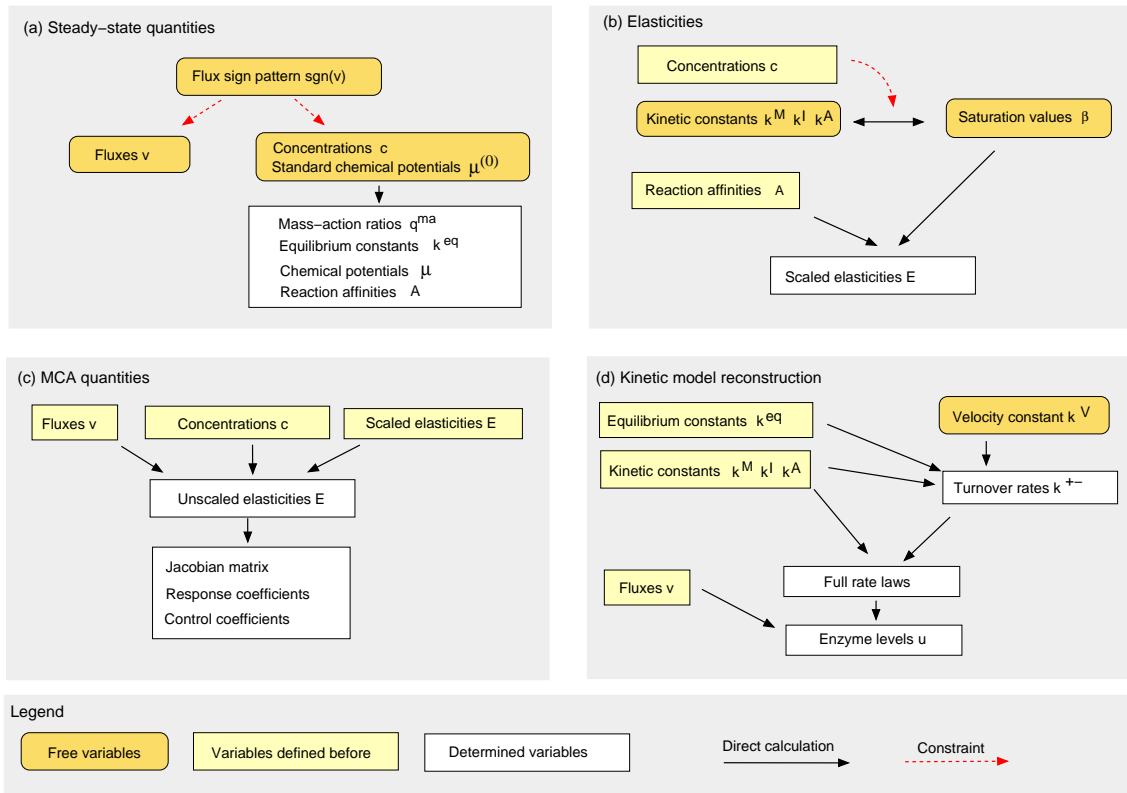


Figure 2: **Dependence scheme for the variables in kinetic steady-state models.** The scheme captures all relevant constraints and can serve as a blueprint for model construction. For clarity, it is shown in four parts. Some model variables can be freely chosen or sampled (yellow), some are determined by others (white), and some are inherited from previous parts (light yellow). (a) Steady-state phase. Fluxes and driving forces need to show the same signs. Given a feasible flux sign pattern, fluxes and chemical potentials can be sampled under linear constraints. (b) Elasticity phase. Saturation values β_{li}^M , β_{li}^A , and β_{li}^I are sampled independently between 0 and 1. Together with the predefined metabolite levels and forces, they determine the dissociation constants (k_{li}^M , k_{li}^A , and k_{li}^I) and the reaction elasticities. These, in turn, determine the control properties (c) and the remaining rate constants and enzyme levels (d).

for a model construction in the spirit of ORACLE and SKM. First, we arrange all model variables (that is, all dynamic variables and the rate constants) in a scheme that describes their dependencies (Figure 2). To construct a model, we just follow the scheme: starting from a network (reaction stoichiometries and allosteric regulation arrows), we choose the state variables (concentrations, fluxes, equilibrium constants), sample the saturation values, and use Eq. (1) to obtain consistent elasticities for the rate laws in question, including second-order elasticities. Among all sampled models, those with a stable reference state can be selected based on their Jacobian matrix. In the resulting “stable” sub-ensemble, the model variables will show other distributions and correlations: even the saturation values, which were sampled independently, may now be dependent. From the second-order elasticities, we obtain second-order control and response coefficients for static [36] or periodic perturbations [39], describing synergisms between enzyme inhibitors. Details about the model construction algorithm are given in Methods and appendix B. The different stages of model construction, for a model of central metabolism in human hepatocytes, our running example, are

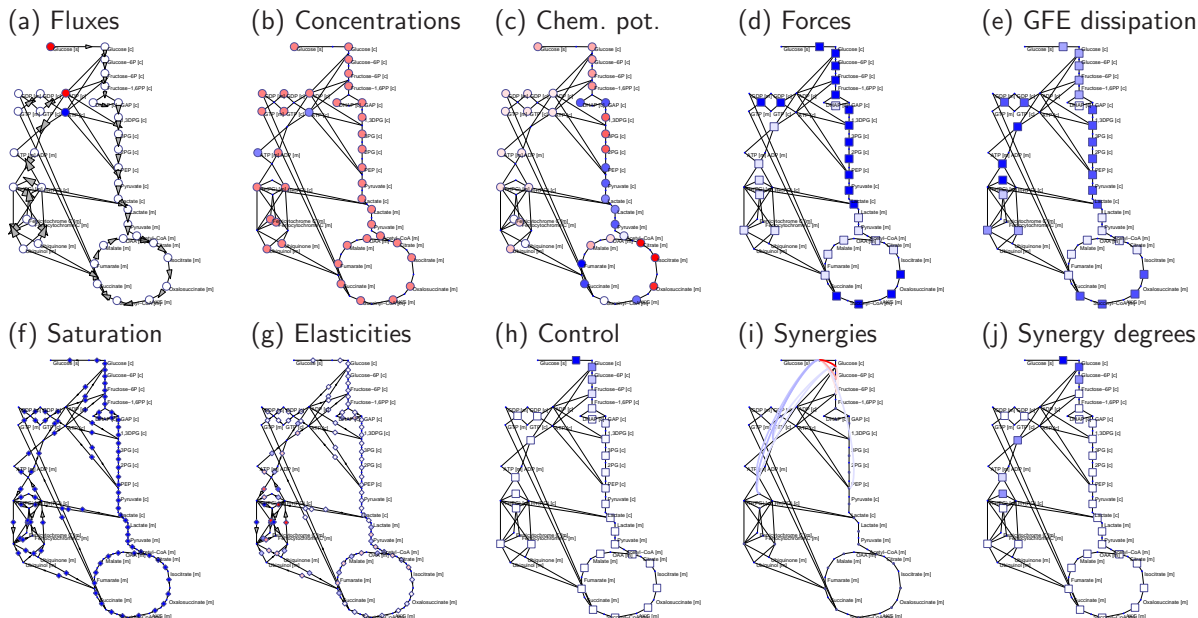


Figure 3: **Construction of a kinetic model step by step.** Model of central carbon metabolism in human liver cells (circles metabolites; arrows or squares: reactions). The network structure was derived from the Hepatonet1 model [40] with a minimal flux distribution for aerobic regeneration of ATP under consumption of glucose. The panels show different model variables, obtained step by step during model construction, for one of the many possible model instances obtainable by elasticity sampling. (a) A thermodynamically feasible flux distribution (grey arrows), obtained by flux minimisation, was taken from [40]. Production and consumption of glucose, ADP and ATP marked by colors. (b) Metabolite levels. (c) Chemical potentials. (d) Thermodynamic driving forces. (e) Local dissipation of Gibbs free energy (driving force multiplied by flux). (f) Saturation values. (g) Scaled elasticities. (h) Control coefficients for ATP production, predicted by elasticity sampling. (i) Synergisms (scaled second-order control coefficients) for ATP production. (j) Synergy degrees (number of substantial synergisms per enzyme). Positive values are shown in blue, negative values in red, zero values in white.

shown in Figure 3. The model was constructed from the whole-genome Hepatonet1 model by selecting a minimal flux mode needed for regeneration of ATP under consumption of glucose and oxygen.

The reconstructed models and their metabolic states satisfy all relevant constraints: flux stationarity, Wegscheider conditions for equilibrium constants and driving forces, Haldane relations for rate constants, and the thermodynamic sign relation between fluxes and driving forces. How do they capture real biological behaviour? As a simple test, we can compare them to established kinetic models with the same network structure and reference state. Appendix G shows two examples, a model of the threonine pathway in *E. coli* [41] and a model of glycolysis in human hepatocytes [42]. With all rate constants being sampled, we cannot expect to reobtain the original model behaviour precisely, but in both cases, the simulations show a realistic qualitative behaviour and realistic time scales.

The model construction can be used to translate metabolic networks into kinetic models and to study the effects of network structure, thermodynamics, and enzyme saturation. By varying factors like network structure, reference fluxes, or rate laws of a model, their effects on metabolic dynamics and control can be

systematically studied. The thermodynamic forces, in particular, have specific effects on global dynamics and control: reactions with large driving forces can act as rectifiers, and the strength of thermodynamic forces can influence control and stability of the metabolic state. The following examples show how the model construction can be used to predict flux control, enzyme synergisms, and metabolic fluctuations propagating in networks, and to assess the impact of thermodynamics on these processes.

2.2 Flux control by enzymes

An enzyme's effect on biomass production, or on other metabolic objectives, can be positive or negative. In FBA, enzyme knock-downs can compromise, but never improve the metabolic objective. In kinetic models, optimality might imply that the control coefficients towards a metabolic objective should be positive, in order to justify the marginal enzyme costs in these reactions. However, this need not be the case mechanistically. In a model, the control coefficients can have either sign, and an enzyme induction may, for instance, inhibit biomass production. Nevertheless, if we build models by elasticity sampling, and if fluxes are taken from flux minimisation under some metabolic objective [14], we find that most of the remaining enzymes exert a positive control on this objective. This is not surprising because of the enzymes that could compromise the objective, some already shut down during flux minimisation.

In our running example (Figure 3), all control coefficients towards ATP regeneration are positive, so all active enzymes support the objective. However, positive control coefficients for a metabolic objective are not generally guaranteed: Figure 4 shows another flux mode, obtained from the same hepatocyte network, but for another objective: anaerobic UTP regeneration under glucose consumption. To construct a simple model, all enzymes were assumed to be half-saturated. The flux control coefficients describe how changes of enzyme levels affect the UTP rephosphorylation rate: surprisingly, the enzyme for UTP rephosphorylation has a negative control C_{uUTP}^{uUTP} , i.e., decreasing this enzyme level will increase its own rate. The same adverse effect becomes visible in dynamic simulations: if the enzyme level is increased, the flux rises immediately, but then drops to a lower steady-state value. If we plot the steady-state flux against the enzyme level, the curve slope in the reference state – i.e., the response coefficient \bar{R}_{uUTP}^{uUTP} – is negative.

The reason is that UTP production tends to reduce the ATP level; due to the turbo design of glycolysis [43], an increasing ATP demand can cause the ATP level to drop dramatically, leading to a strong decrease in UTP rephosphorylation. In contrast, a lower UTP production would allow ATP to recover, and the gain in ATP level could overcompensate the lower enzyme activity in UTP production. Is this behaviour, which occurs for half-saturated enzymes, a general feature of this flux mode? Elasticity sampling can help us find out. In a model ensemble with randomly drawn saturation values, about 90 percent show a negative response coefficient \bar{R}_{uUTP}^{uUTP} . Therefore, we can attribute the self-repression, at least partially, to the combination of fluxes and thermodynamic forces. to test this again, all driving forces were varied proportionally: if all reactions come close to equilibrium, the self-repression disappears; if they are made even more irreversible, the self-repression becomes stronger.

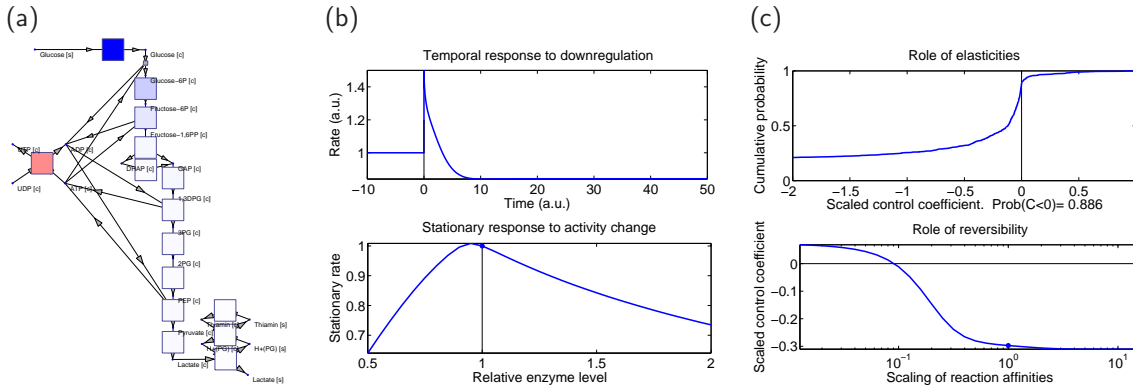


Figure 4: **Adverse effect of enzyme regulation.** (a) Flux distribution in human liver cells performing anaerobic rephosphorylation of UTP. Flux distribution, obtained by flux minimisation, taken from [40]. Flux control coefficients (blue: positive; pink: negative) were obtained by setting all saturation values to 0.5. Paradoxically, UTP rephosphorylation is effectively inhibited by its own enzyme. (b) Model dynamics and control. Top: induction of the UTP-producing enzyme first speeds up the reaction, but eventually the rate is decreased. Bottom: dose-response curve between enzyme level (x-axis) and stationary UTP production rate. In the reference state (marked by line), the response coefficient, given by the curve slope, is negative. (c) Dependence on saturation and driving forces. Top: Cumulative distribution of the self-response coefficient, obtained from a random sampling of saturation values (uniformly between 0 and 1). In about 90 percent of the model instances, the control remains negative. Bottom: The self-response coefficient depends on the thermodynamic forces. As all driving forces are increased by a common factor (shown on x-axis), the self-response (y-axis) becomes more negative (all saturation values set to 0.5).

2.3 Enzyme synergies

If an enzyme's influence on some output variable is altered by other enzyme perturbations, this is called a synergism (or antagonism, in the case of a negative synergisms). To quantify a synergism, we consider two perturbation parameters (e.g., enzyme activities) and an output variable (e.g., the growth rate in microbes). If two separate perturbations change the output by factors w_a or w_b (typically smaller than 1 if the output is a metabolic objective), the double perturbation could be expected to cause a change $w_a \cdot w_b$. Given the observed change w_{ab} , which may be larger or smaller, we define the synergy $\eta_{ab}^z = \ln \frac{w_{ab}}{w_a w_b}$. If we expect additive instead of multiplicative effects, the difference $\bar{\eta}_{ab}^z = w_{ab} - (w_a + w_b)$ is a suitable synergy measure. Any factors that affect the reaction rates can show synergisms: enzyme inhibitors, knock-outs, differential expression, or changes in metabolic supply and demand.

For small perturbations in kinetic models, synergisms can be predicted by MCA. While normal control coefficients capture the linear effects of single enzymes, second-order control coefficients capture enzyme-pair synergies. With enzyme changes $\Delta \ln u_a$ and $\Delta \ln u_b$ and the above definition, the synergy $\eta_{ab}^z \approx R_{u_a u_b}^z \Delta \ln u_a \Delta \ln u_b$ is determined by scaled second-order control coefficients $R_{u_a u_b}^z$, which we shall call "synergy coefficients". In the case of double inhibitions, negative synergies ($R_{u_a u_b}^z < 0$) are aggravating, while positive synergies ($R_{u_a u_b}^z > 0$) are buffering; for double activations, the opposite holds. In contrast to FBA or full kinetic simulations, where perturbations are simulated one by one, MCA yields the second-order elasticity matrix directly from the second-order elasticities, which can be sampled as described (see appendix B and I.2).

The reason for synergisms in MCA can be understood as follows: in a kinetic model, a first inhibition is likely to change the flux control coefficients of all enzymes, and therefore the effects of a second inhibition. Self-synergies (for a two-fold inhibition of a single enzyme) are typically aggravating: the first inhibition increases the enzyme’s control, which makes a second inhibition have stronger effects on the output. The synergies predicted by MCA show some expected patterns (for an example, see appendix E): (i) synergies between cooperating enzymes (within a linear pathway) tend to be buffering, while synergies between alternative pathways tend to be aggravating; (ii) synergies between different pathways tend to be monochromatic, i.e., their signs depend on the pathways, not on the specific enzymes perturbed within them; (iii) enzymes with large single-enzyme influences also tend to show larger (positive or negative) synergies. The quantitative synergies depend, of course, on rate laws, enzyme saturation, and allosteric regulation.

How does this compare to predictions from constraint-based methods like FBA or MoMA? In FBA, synergies for small or large flux perturbations, can be computed as follows. We start from an FBA problem with a given objective (e.g. biomass production flux) and accept its solution as the reference state. To perturb one of the reactions, we impose an upper flux bound on this reaction, given by a fraction $0 \leq \lambda < 1$ of its reference flux. After applying one or two perturbations, we can solve the FBA problem again and obtain a perturbed objective value. Perturbations in MoMA can be simulated accordingly. Although flux analysis and MCA are based on different assumptions (flux optimisation in FBA; flux buffering in MoMA; and mechanistic response in MCA), the synergisms show some common patterns, probably caused by the network structure and reference fluxes. For a small example pathway (Figure 5), MCA predicts more, and more gradual synergies than FBA, whereas MoMA ranges in between. In FBA, double enzyme repressions in linear chains are combined by a “min” function: after a first inhibition, the second inhibition will either retain its full effect, or have no effect at all, entailing in both cases strongly buffering synergies. To obtain comparable positive and negative epistasis values from FBA calculations, Segré *et al.* [44] introduced a numerical correction specifically for buffering interactions (see appendix E). With MCA, such a correction is not necessary because positive and negative synergy values are on the same order of magnitude.

Unlike FBA or MoMA, MCA does not only yield numerical predictions, but explicit formulae for synergies, which may clarify some patterns observed. For instance, the scaled second-order control coefficients depend on three factors (see Eq. (49) in appendix I.2): on the first-order flux control C_v^j between both reactions; on the first-order control C_u^y between the reactions and the output; and on the second-order elasticities of all reactions. This suggests that a large control between reactions and objective, and between both reactions, makes large synergies (either positive or negative) more likely. Furthermore, MCA does not distinguish between enzyme knock-outs, enzyme-inhibiting drugs, or other different types of perturbation that decrease an enzyme activity. A synergy prediction may equally concern pairs of enzyme knock-downs, pairs of enzyme-inhibiting drugs, or combinations of both. This agrees with the finding that genes with many epistasis partners are more likely to show gene-drug interactions [45].

2.4 Metabolic fluctuations

Metabolite levels and fluxes can vary both between cells and in time. Fluctuations originate in individual reactions from varying enzyme levels, changes of supply and demand, or from chemical noise and lead to metabolite or flux fluctuations everywhere in the network. On the one hand, variation may be slow or even

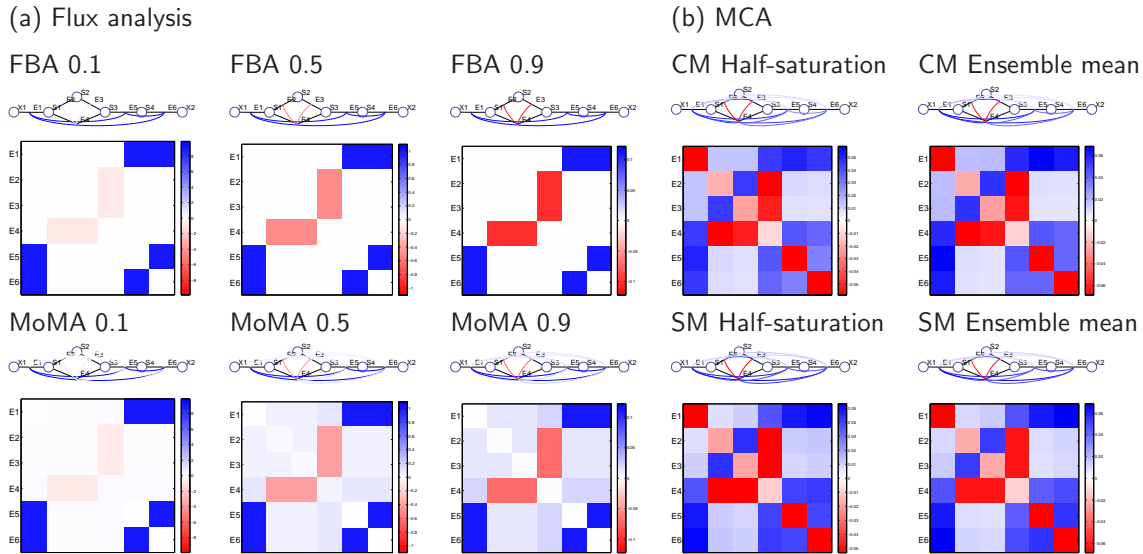


Figure 5: **Synergies in a simple example pathway.** The pathway is a linear chain with two parallel routes between the intermediates S1 and S3. (a) Synergies computed by flux analysis. Synergies for double inhibitions are shown by arc colours (red: aggravating, blue: buffering). The panels show synergies computed by different methods (top: FBA; bottom: MoMA) and three inhibition strengths (by factors of 0.1, 0.5, and 0.9.). Double inhibitions of one enzyme are multiplicative, i.e., leading to inhibition strengths of 0.01, 0.25, and 0.81, respectively. Color scales are adjusted to maximal cross-enzymes value per panel, small values (smaller than one percent of the maximal absolute value) are not shown. (b) Synergies computed by MCA. The four pictures show results from different rate laws (CM: common saturable rate law; SM: simultaneous-binding modular rate law) and compares the results from half-saturation to mean values from model ensembles with randomly chosen saturation. The results are almost identical.

static, representing differences between cells. In this case, enzyme levels can be modelled as quasi-static. Their variation in the ensemble defined by the random parameter perturbations is described by a covariance matrix $\mathbf{cov}(\mathbf{p})$, and the resulting variation in metabolite levels by a covariance matrix $\mathbf{cov}(\mathbf{c})$. For small variances, it can be approximated by $\mathbf{cov}(\mathbf{c}) \approx \mathbf{R}_p^s \mathbf{cov}(\mathbf{p}) \mathbf{R}_p^{s\top}$ using the response coefficient matrix $\bar{\mathbf{R}}_u^s$, and the approximation can be improved by second-order response coefficients [24] (for an example, see Figure 6). Analogous formulae hold for variation in fluxes. On the other hand, dynamic fluctuations can be caused by fast perturbations or chemical noise, which originate in individual reactions, propagate through the network, and cause dynamic fluctuations of metabolites and fluxes, our observable outputs. To model their dynamic, we can characterise them by spectral power densities, which, for small noise amplitudes, follow from the elasticities (see Eq. (31) in appendix).

Chemical noise in cell metabolism arises from fluctuations in reaction rates. The order of magnitude of this noise can be roughly estimated: A typical enzyme (with 1000 copies in a bacterial cell and $k^{\text{cat}} = 10 \text{ s}^{-1}$) produces a flux of 10^4 molecules per second. If we neglect the reverse flux and assume that the number of reaction events per second is Poisson distributed, the typical fluctuation of these 10^4 events per second should be around 10^2 , that is, about one percent. For smaller time intervals, this percentage will become larger and for larger time intervals, smaller. How does the noise at the source translate into actual metabolite fluctuations? To answer this, we need to consider how noise propagates through

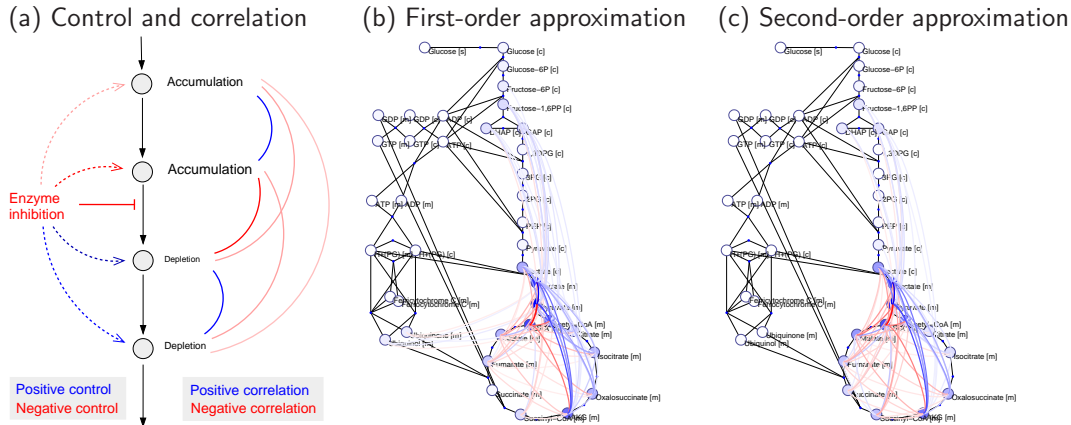


Figure 6: **Static metabolite variation.** (a) The effect of an enzyme inhibition (left, solid arrow) is described by response coefficients (dotted arrows). A variation of the enzyme level leads to correlated metabolite fluctuations (arcs on the right, blue: positive; red: negative). (b) Correlated variation of metabolite levels in hepatocyte central metabolism (appendix G). Metabolite variation caused by an equal, uncorrelated variation of all enzyme levels (standard deviation of logarithmic enzyme levels: $\log 2$). Metabolite variances (circles) and covariances (arcs) computed from first-order approximation. (c) The second-order approximation changes the result only slightly.

the network, how it is damped (or possibly amplified), and how noise from different sources adds to the observable, correlated metabolite fluctuations. In the chemical Langevin equation [46], noise at the source is approximated by white noise containing all frequencies with equal amplitudes, and the linearised model acts as a linear filter that translates the original noise spectrum into the noise spectrum of the metabolite levels. The noise amplitude at the source reaction increases with the component rates v^+ and v^- . Close to chemical equilibrium, the microscopic rates almost cancel each other, but will be large individually and therefore produce stronger noise. Irreversible reactions, on the contrary, produce less chemical noise and serve as rectifiers for its propagation. Both the origin and the transmission of noise depends on thermodynamic forces. Figure 7 shows, as an example, correlated metabolite fluctuations in hepatocyte central metabolism, our running example. In the simulations, high-frequency fluctuations represent direct, non-stationary effects close to the noise source, whereas low-frequency noise represents global, almost stationary shifts of the flux distribution which have evaded the filtering by the system dynamic.

2.5 Dynamics and control reflect network structure and thermodynamics

Observed flux control, synergisms and differential expression show characteristic patterns in the metabolic networks, which reflect functional associations between enzymes, in particular their arrangement along metabolic pathways [47]. Also metabolite fluctuations may reflect the network structure [48]. However, the patterns do not portray the network structure directly. MCA, combined with elasticity sampling, shows how other factors – thermodynamics, saturation, and allosteric regulation – come into play, and how the sparse network adjacency matrix relates to the rather extended patterns. One can argue that enzyme control and synergies, metabolite fluctuations, and possibly optimal differential expression patterns

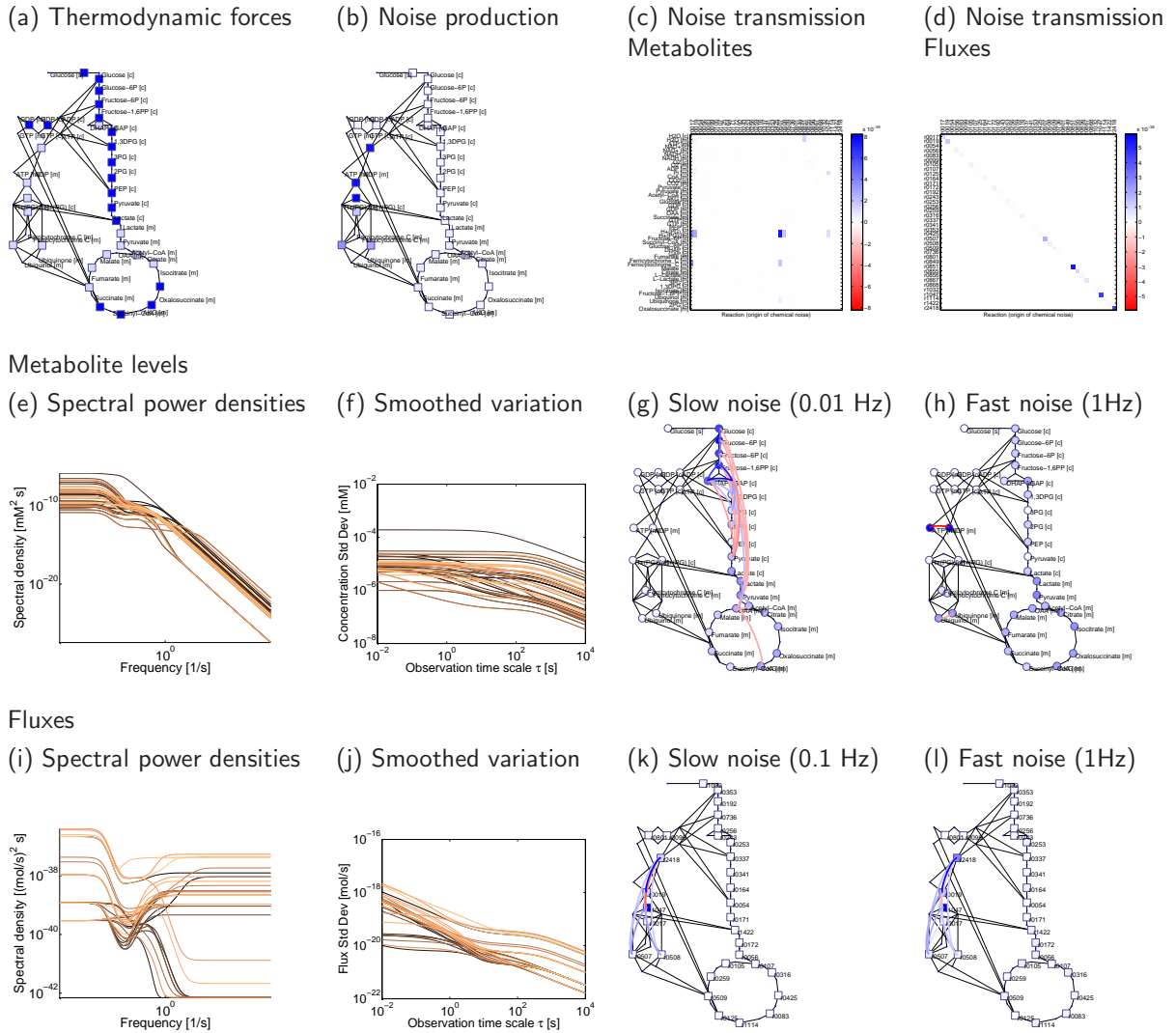


Figure 7: **Metabolite fluctuations caused by chemical noise.** (a) Thermodynamic driving forces in hepatocyte glycolysis (appendix G), with a cell volume of $10000 \mu\text{m}^3$ and a glycolytic flux of $1 \text{ mM}/\text{min}$. (b) Reactions near equilibrium (small driving forces) produce stronger chemical noise because of their large microscopic fluxes. Power density of original noise (Eq. (32) in appendix; shown by shades of blue) is concentrated in the respiration reactions on the left. Panels (c) and (d) show transmission between noise sources (reactions in which chemical noise emerges) and metabolite levels or fluxes (where fluctuations are observed), at a frequency of 1 Hertz. Noise transmission is quantified by the squared spectral response coefficient, summed over forward and backward direction of the source reaction. (e) Noise in metabolite levels. Metabolite fluctuations (square roots of spectral power densities) decrease with the frequency. Each curve corresponds to one metabolite. (f) Smoothing, with a certain time resolution, decreases the variance of metabolite fluctuations. At lower time resolutions, high-frequency fluctuations are filtered out (see appendix I.3). The curves show the variability of metabolite levels (y-axis), as computed for different time resolutions (x-axis). (g) Low-frequency metabolite fluctuations are correlated all over the pathway. Circles colors show spectral power densities at 0.01 Hertz, arc colors the covariances (blue: positive; red: negative). (h) High-frequency metabolite fluctuations (1 Hertz) are concentrated close to the noise source reaction. Panels (i) - (l) show analogous results for flux fluctuations.

[37] reflect some types of response coefficients. These, in turn, depend on network structure, fluxes, concentrations, and on the reaction elasticities. Stoichiometric matrix and elasticity matrix determine the control properties in an indirect way: their product $\mathbf{N}^{\text{int}} \bar{\mathbf{E}}$ is the Jacobian which, by its sparsity structure, links neighbouring compounds and therefore represents the local network topology. Control and response coefficients are based on the *inverse* Jacobian and are therefore non-sparse matrices, describing global, extended effects in the entire network.

As we saw, chemical noise can show both extremes: high-frequency noise tends to portray the local neighbourhood of the source reaction, while low-frequency is as extended as the stationary flux modes. The theorems of MCA [49] yield another link between local structure and global behaviour: the sum of control coefficients along a stationary flux is determined by the network structure (summation theorem), while the control coefficients around metabolites are constrained by the local elasticities (connectivity theorem). Thus, network structures shape the dynamics, but only together with the elasticities, which can be explored by elasticity sampling.

Predefined by the reference state, the thermodynamic forces have a number of dynamic effects both within their reactions and on the global dynamic. Within the reactions, large forces entail a larger dissipation of Gibbs free energy and a smaller reverse flux. With a net flux predefined, this reduces the microscopic fluxes v^{\pm} and thus the production of chemical noise. If there is little backward flux, the enzyme works efficiently and the enzyme demand is low. Moreover, the net rate becomes insensitive to the product level, decreasing the flux control of downstream enzymes and thereby increasing the enzyme's own control. This would make an enzyme a suitable regulation point. If, in contrast, a reaction's driving force is large, reverting the flux requires large concentration changes and a flux reversal is difficult or impossible. In addition, the driving force, together with the flux, defines a typical time scale for relaxation of imbalances. The patterns of thermodynamic forces can shape global flux control. Consider a linear pathway in which one reaction is irreversible (with a very large driving force). Since the reaction is not slowed down by product accumulation, it acts as a rectifier for metabolic perturbations. The reaction has full flux control and the downstream enzymes have no impact on the flux. Similar, but less extreme effects would pertain for a large, but finite thermodynamic force. The effects of force and saturation in a linear chain are systematically studied in appendix Figure 11.

3 Discussion

A systematic use of constraints can help to build meaningful models even when data are scarce, and to discard models that describe a *perpetuum mobile*. Dependence schemes, as shown in Figure 2, make constraints applicable for model construction no matter if variables are sampled, fitted, optimised, or manually chosen. The conditional sampling and the independencies claimed in the scheme raise concerns as to which biochemical parameters are actually independent, or conditionally independent, during the life of a cell, between cells in a population, or during evolution. For instance: can the Michaelis constants and the forward catalytic constant of enzymes be varied independently, with the reverse catalytic constant depending on them, or should forward and reverse catalytic constants be chosen independently? Should catalytic constants rise with the enzyme levels (because both are under selection for high enzyme capacity),

or should the opposite hold (because very efficient enzymes do not require large amounts)? Comprehensive kinetic and metabolic data, needed to study biochemical dependencies empirically [50], are only beginning to emerge, and our dependence scheme represents one pragmatic solution.

In the present approach, just like in ORACLE or SKM, a metabolic state is chosen first and its control properties are determined later conditionally. Such a stepwise choice can also be a way to think of optimisation in evolution or biotechnology: on the one hand, cells may have to optimise fluxes and concentrations under standard external conditions; on the other, this state must be stabilised or made adaptable to external changes. In evolution, thermodynamics and kinetics provide distinct ways to adjust metabolic control patterns. An ATP investment, for instance, can turn a reaction into a rectifier for fluxes and signals (i.e., perturbations and noise) and, at a fixed net flux v , reduce noise production. If the reactant levels are seen as optimised – and the thermodynamic forces are therefore fixed – the elasticities can still be modified by tweaking the saturation levels or adding allosteric regulation between virtually any reaction and any compound. To maintain the fluxes, the incomplete enzyme efficiency needs to be compensated by higher enzyme levels, so allosteric regulation entails a permanent enzyme cost. In a more traditional modelling, where kinetic models are predefined solved for a steady state numerically, state and control appear entangled and their optimisation is harder to understand.

Control coefficients obtained by elasticity sampling can be used to predict flux changes after perturbation. While FBA predicts most favourable flux changes, and MoMA yields the least noticeable ones, MCA predicts them from a biochemical model. In flux analysis methods like FBA and MoMA, enzyme repression is modelled by restricting a reaction flux to smaller values (knock-down) or to zero (knock-out), and a new flux profile is chosen by maximising a metabolic objective (in FBA) or by requiring minimal flux changes (in MoMA). Enzyme repressions in a linear pathway, are effectively combined by a `min` function, which entails strong buffering interactions. In reality, enzyme inhibitions will gradually change the control patterns within a pathway. The resulting quantitative synergies are captured by MCA, with precise numbers depending on enzyme saturation and allosteric regulation. In particular, reactions are not completely reversible or irreversible, as in FBA, but may show various degrees of reversibility depending on the thermodynamic force. The quantitative effects, e.g. for the transmission of perturbations, can be systematically studied (an example is given in appendix G). Of course, MCA has some limitations: on the one hand, the predictions are only valid for small perturbations. On the other, permanent perturbations would cause cells to adapt their enzyme levels by expression changes. The effects of such adaptations are of second order, so they may be neglected for small perturbations. If the perturbations are larger, known enzyme adaptations could be incorporated in the calculation, and unknown ones could be predicted based on MCA and optimality principles [37].

Sampling can also be used to adjust models to specific experimental data: if kinetic, thermodynamic, or metabolic data are available [51, 52], they can be inserted, used to define bounds, or treated as mean values in sampling. For a global variability analysis, model variables could be drawn from broad distributions, reflecting plausible parameter ranges [53, 18, 50]. Model ensembles that reflect subjective uncertainty or biological variability can be screened for quantitative outputs or types of dynamic behaviour. Automatically built models do not reach the quality of manually made ones, but they could serve as scaffolds into which high-quality reaction or pathway models can be inserted: Linearised and automatically reduced to simple

black-box models [32], they could provide pathways of interest with realistic dynamic boundaries. The resulting models help to understand the global interplay between fluxes, metabolite levels, and transcript levels, to simulate periodic perturbations and noise [39], and to predict optimal enzyme adaption to changing supply and demand or to enzyme-inhibiting drugs [37].

4 Methods

Elasticities and linearised models A description of kinetic models, their thermodynamic and kinetic properties, MCA, and the mathematical symbols used is given in appendix B. Linearised models can be directly built from the reaction stoichiometries and from the reaction elasticities in a reference state. In a linear approximation, the fate of a metabolic perturbation vector $\Delta c(t)$ is described by linear differential equations $\frac{d}{dt} \Delta c(t) = \mathbf{J} \Delta c$ where the Jacobian matrix $\mathbf{J} = \mathbf{N}^{\text{int}} \bar{\mathbf{E}}$ contains the elasticity matrix $\bar{\mathbf{E}}$. By solving the linearised equations, one can trace small dynamic perturbations in the network. An enzyme inhibition, for instance, will make the substrate accumulate and deplete the product. This has secondary effects which typically counteract the original effect and, eventually, shift fluxes and concentrations across the network. Elasticities, which describe the immediate effect of metabolite perturbations on reaction rates, are the key to modelling biochemical systems close to steady state.

Elasticities of the modular rate laws The modular rate laws (see [19] and appendix C) are a family of general reversible rate laws, representing simple enzymatic mechanisms and comprising reversible mass-action and Michaelis-Menten kinetics as special cases. Their scaled elasticities can be split in two terms [19]:

$$E_{c_i}^{v_l} = E_{l_i}^{\text{rev}} + E_{l_i}^{\text{kin}}, \quad (1)$$

where the thermodynamic term $E_{l_i}^{\text{rev}}$ depends only on the driving forces A_l , while the kinetic term $E_{l_i}^{\text{kin}}$ depends on enzyme saturation and allosteric regulation. A full description of the modular rate laws, as well as their first- and second-order elasticities, is given in [19] and its supplementary information.

Thermodynamic elasticity term The thermodynamic term follows from the typical mass-action-like numerator, common to many reversible rate laws, and reads [19]

$$E_{l_i}^{\text{rev}} = \frac{v_l^+ m_{l_i}^+ - v_l^- m_{l_i}^-}{v_l} = \frac{\zeta_l m_{l_i}^+ - m_{l_i}^-}{\zeta_l - 1} \quad (2)$$

with the flux ratios $\zeta_l = \frac{v_l^+}{v_l^-} = e^{h_l A_l / RT}$, the cooperativity exponent h_l of the rate law, the driving force $A_l = -\Delta_r G_l$ Boltzmann's gas constant R , and the absolute temperature T . For reactions close to equilibrium and with positive fluxes (i.e., small positive driving forces $A_l \approx 0$), the term for substrates (where $m_{l_i}^+ > 0$, $m_{l_i}^- = 0$) approaches infinity and the term for products (where $m_{l_i}^+ = 0$, $m_{l_i}^- > 0$) approaches $-\infty$. For almost irreversible reactions (driving force $A_l \rightarrow \infty$), the terms approach $m_{l_i}^+$ (for substrates) and 0 (for products). For a small driving force of 1 kJ/mol $\approx 0.4 RT$, the values are about 3 for substrates and -2 for products (with cooperativity coefficient and stoichiometric coefficients equal to

1); for a larger driving force of 10 kJ/mol, we obtain 1.02 (substrate) and -0.02 (product).

Kinetic elasticity term The kinetic elasticity term $E_{i_i}^{\text{kin}}$ depends on the type of rate laws. For the modular rate laws, it can be computed from the saturation values $\beta_{i_i}^X = c_i / (c_i + k_{i_i}^X)$, which describe the saturation of enzymes with reactants or modifiers. Here, c_i is a metabolite level, $k_{i_i}^X$ is the dissociation constant between metabolite and enzyme, and X stands for M (reactants), A (activators), or I (inhibitors). The saturation values range between 0 and 1 and, given the metabolite levels, determine the dissociation constants. For the simultaneous-binding modular (SM) rate law with non-competitive allosteric activation and inhibition [19], the kinetic elasticities comprise four additive terms, describing the influences of substrates, products, activators, and inhibitors:

$$E_{c_i}^{v_i} = E_{i_i}^{\text{rev}} - [m_{i_i}^+ \beta_{i_i}^M + m_{i_i}^- \beta_{i_i}^M] + [m_{i_i}^A (1 - \beta_{i_i}^A) - m_{i_i}^I \beta_{i_i}^I]. \quad (3)$$

In other rate laws, and with non-competitive allosteric regulation, the kinetic elasticity terms can be further split into $E_{i_i}^{\text{reg}} - E_{i_i}^{\text{sat}}$, where $E_{i_i}^{\text{reg}}$ stems from the prefactor for allosteric regulation, and $E_{i_i}^{\text{sat}}$ from the rate law's denominator.

In a mass-action or power-law rate law without allosteric regulation, the term $E_{i_i}^{\text{kin}}$ vanishes and the elasticities are directly determined by the driving forces:

$$\mathbf{E} = \text{Dg}(\mathbf{v})^{-1} [\text{Dg}(\mathbf{v}^+) \mathbf{M}^+ - \text{Dg}(\mathbf{v}^-) \mathbf{M}^-] = \text{Dg}(\zeta - \hat{1})^{-1} [\text{Dg}(\zeta) \mathbf{M}^+ - \mathbf{M}^-], \quad (4)$$

so no further sampling is needed. Formulae for the common saturable rate law – a modified version of the convenience kinetics – and for other rate laws and second-order elasticities are given in [19] and in appendix I.5. The elasticity formula in Structural Kinetic Modelling,

$$E_{c_i}^{v_i} = m_{i_i}^+ (1 - \beta_{i_i}^M) + m_{i_i}^A (1 - \beta_{i_i}^A) - m_{i_i}^I \beta_{i_i}^I, \quad (5)$$

resembles Eq. (3). Both formulae become identical for the limiting case of irreversible reactions (where $m_{i_i}^+ = 0$ and $E^{\text{rev}} m_{i_i}^+$). Since the elasticities depend on the driving forces, and these can be coupled by Wegscheider conditions, all elasticities in a model may be dependent. However, given the driving forces and metabolite levels, the saturation values are physically unconstrained (proof see appendix C), and the elasticity formula (1) yields consistent elasticities for the specified rate law.

Sampling algorithm Models can be constructed by following the dependence scheme in Figure 2. The free variables of a model can be sampled, chosen manually, fitted to data, or optimised. Each set of elasticities leads to consistent rate constants, and can therefore be realised by a consistent kinetic model with defined reversible rate laws. Just like ORACLE and SKM, the procedure consists of three phases: In the steady-state phase, we choose thermodynamically feasible fluxes, metabolite levels, and equilibrium constants (or possibly, the Gibbs free energies of formation), which determine the chemical potentials and driving forces. The state variables can be sampled or chosen by any method for thermodynamic flux analysis. In the elasticity phase, saturation values are sampled independently in the range $]0, 1[$, and the elasticity matrix is computed by Eq. (1). In the MCA phase, we compute variables like unscaled elasticities $\bar{E}_{c_i}^{v_i}$, rate constants, the Jacobian matrix, response and control coefficients, or properties like the stability

of the steady state. The algorithm is described in appendix D and MATLAB code for elasticity sampling is freely available at https://github.com/wolframliiebermeister/elasticity_sampling.

For the simultaneous-binding modular rate law, Eq. (1) yields the same sampling scheme as SKM except for the thermodynamic term E_{ii}^{rev} , which makes the elasticities dependent and thermodynamically consistent. With other rate laws, the formula changes, but the simple sampling strategy remains. A variant of the algorithm can be used to build kinetic models with multiple steady states: in the steady-state phase, a single set of equilibrium constants and several sets of fluxes and concentrations for different steady states are chosen; in the elasticity phase, dissociation constants (k_{ii}^{M} , k_{ii}^{A} , and k_{ii}^{I}) and velocity constants k_l^{V} (geometric means of forward and reverse catalytic constants) are chosen, for instance, by parameter balancing [54, 22]. Enzyme levels and elasticities are computed afterwards by matching the reaction rates to the predefined fluxes. If the dissociation constants k_{ii}^{M} , and not the saturation values, are independently sampled, they will be statistically independent of the compound concentrations and less likely to match their orders of magnitude.

Model ensembles The sampled model instances form a statistical ensemble which reflects the network structure and the choices made by the modeller, while other variables remain uncertain. Different model assumptions or model variants can be implemented by distinct model ensembles. Suitable distributions for sampling are uniform distributions or beta distributions (for saturation values) or log-normal distribution (for rate constants). To study how certain model features influence the dynamics, one may realise model variants by different model ensembles and screen them for significant differences in the over the sampled modelsir behaviour (for details on the significance tests, see appendix H.2). For instance, one can check how network structure, thermodynamics, enzyme saturation and allosteric regulation stabilise or destabilise steady states, assess the values and signs of control coefficients or synergies, compute their distributions and correlations, and check which control coefficients are significantly different from zero. All predictions are probabilistic, reflecting the uncertainties arising from incomplete and inaccurate data. Although no kinetic data are needed for building a model, known rate constants can be used to make a model ensemble more precise. In this way, data that would not suffice for model fitting can still be used to obtain a model ensemble, whose uncertainties can be assessed statistically.

Acknowledgements

The author thanks Ronan Fleming, Edda Klipp, Elad Noor, Tomer Shlomi, and Ralf Steuer for inspiring discussions. This work was funded by the German Research Foundation (LI 1676/2-1).

References

- [1] S.M. Fendt, J.M. Büscher, F. Rudroff, P. Picotti, N. Zamboni, and U. Sauer. Tradeoff between enzyme and metabolite efficiency maintains metabolic homeostasis upon perturbations in enzyme capacity. *Mol. Sys. Biol.*, 13(6):356, 2010.

- [2] N. Ishii, K. Nakahigashi, T. Baba, M. Robert, T. Soga, A. Kanai, T. Hirasawa, M. Naba, K. Hirai, A. Hoque, P. Yee Ho, Y. Kakazu, K. Sugawara, S. Igarashi, S. Harada, T. Masuda, N. Sugiyama, T. Togashi, M. Hasegawa, Y. Takai, K. Yugi, K. Arakawa, N. Iwata, Y. Toya, Y. Nakayama, T. Nishioka, K. Shimizu, H. Mori, and M. Tomita. Multiple high-throughput analyses monitor the response of *E. coli* to perturbations. *Science*, 316(5824):593 – 597, 2007.
- [3] A.M. Feist, C.S. Henry, J.L. Reed, M. Krummenacker, A.R. Joyce, P.D. Karp, L.J. Broadbelt, V. Hatzimanikatis, and B.Ø. Palsson. A genome-scale metabolic reconstruction for *Escherichia coli* K-12 MG1655 that accounts for 1260 ORFs and thermodynamic information. *Molecular Systems Biology*, 3:121, 2007.
- [4] C.S. Henry, M. DeJongh, A.A. Best, P.M. Frybarger, B. Linsay, and R.L. Stevens. High-throughput generation, optimization and analysis of genome-scale metabolic models. *Nature Biotechnology*, 28:977–82, 2010.
- [5] N.D. Price, J. Schellenberger, and B.Ø. Palsson. Uniform sampling of steady-state flux spaces: Means to design experiments and to interpret enzymopathies. *Biophysical Journal*, 87:2172–2186, 2004.
- [6] D. A. Beard, S. Liang, and H. Qian. Energy balance for analysis of complex metabolic networks. *Biophysical Journal*, 83(1):79–86, 2002.
- [7] A. Kümmel, S. Panke, and M. Heinemann. Putative regulatory sites unraveled by network-embedded thermodynamic analysis of metabolome data. *Molecular Systems Biology*, 2:2006.0034, 2006.
- [8] C.S. Henry, M.D. Jankowski, L.J. Broadbelt, and V. Hatzimanikatis. Genome-scale thermodynamic analysis of *E. coli* metabolism. *Biophys. J.*, 90:1453–1461, 2006.
- [9] A. Hoppe, S. Hoffmann, and H. Holzhütter. Including metabolite concentrations into flux-balance analysis: Thermodynamic realizability as a constraint on flux distributions in metabolic networks. *BMC Syst. Biol*, 1(1):23, 2007.
- [10] D.A. Fell and J.R. Small. Fat synthesis in adipose tissue. An examination of stoichiometric constraints. *Biochem. J.*, 238:781–786, 1986.
- [11] A. Varma and B.Ø. Palsson. Metabolic flux balancing: basic concepts, scientific and practical use. *Biotechnology*, 12:994–998, 1994.
- [12] D. Segrè, D. Vitkup, and G.M. Church. Analysis of optimality in natural and perturbed metabolic networks. *Proc Natl Acad Sci USA*, 99(23):15112–15117, 2002.
- [13] T. Shlomi, O. Berkman, and E. Ruppin. Constraint-based modeling of perturbed organisms: A room for improvement. In *Proceedings of ISMB 2004*, 2004.
- [14] H. Holzhütter. The principle of flux minimization and its application to estimate stationary fluxes in metabolic networks. *Eur. J. Biochem.*, 271(14):2905–2922, 2004.
- [15] R. Schuetz, L. Kuepfer, and U. Sauer. Systematic evaluation of objective functions for predicting intracellular fluxes in *Escherichia coli*. *Molecular Systems Biology*, 3:119, 2007.

- [16] M.A. Savageau. Biochemical systems analysis. III. Dynamic solutions using a power-law approximation. *J. Theor. Biol.*, 26(2):215–226, 1970.
- [17] D. Visser and J.J. Heijnen. Dynamic simulation and metabolic re-design of a branched pathway using linlog kinetics. *Metab Eng*, 5(3):164–176, 2003.
- [18] W. Liebermeister and E. Klipp. Bringing metabolic networks to life: convenience rate law and thermodynamic constraints. *Theor. Biol. Med. Mod.*, 3:41, 2006.
- [19] W. Liebermeister, J. Uhlenendorf, and E. Klipp. Modular rate laws for enzymatic reactions: thermodynamics, elasticities, and implementation. *Bioinformatics*, 26(12):1528–1534, 2010.
- [20] K. Smallbone, E. Simeonidis, N. Swainston, and P. Mendes. Towards a genome-scale kinetic model of cellular metabolism. *BMC Systems Biology*, 2010.
- [21] P. Li, J.O. Dada, D. Jameson, I. Spasic, N. Swainston, et al. Systematic integration of experimental data and models in systems biology. *BMC Bioinformatics*, 11:582, 2010.
- [22] N.J. Stanford, T. Lubitz, K. Smallbone, E. Klipp, P. Mendes, and W. Liebermeister. Systematic construction of kinetic models from genome-scale metabolic networks. *Under review*.
- [23] A. Flamholz, E. Noor, A. Bar-Even, W. Liebermeister, and R. Milo. Glycolytic strategy as a tradeoff between energy yield and protein cost. *PNAS*, 2013.
- [24] W. Liebermeister and E. Klipp. Biochemical networks with uncertain parameters. *IEE Proc. Sys. Biol.*, 152(3):97–107, 2005.
- [25] L. Mišković and V. Hatzimanikatis. Modeling of uncertainties in biochemical reactions. *Biotechnology and Bioengineering*, 108(2):413–423, 2011.
- [26] L. Wang, I. Birol, and V. Hatzimanikatis. Metabolic control analysis under uncertainty: Framework development and case studies. *Biophysical Journal.*, 87(6):3750–3763, 2004.
- [27] L. Wang and V. Hatzimanikatis. Metabolic engineering under uncertainty. I: Framework development. *Metabolic engineering*, 8:133–141, 2006.
- [28] L. Wang and V. Hatzimanikatis. Metabolic engineering under uncertainty. II: Analysis of yeast metabolism. *Metabolic engineering*, 8:142–159, 2006.
- [29] K.C. Soh, L. Miskovic, and V. Hatzimanikatis. From network models to network responses: integration of thermodynamic and kinetic properties of yeast genome-scale metabolic networks. *FEMS Yeast Research*, 12:129–143, 2012.
- [30] R. Steuer, T. Gross, J. Selbig, and B. Blasius. Structural kinetic modeling of metabolic networks. *Proc Natl Acad Sci USA*, 103(32):11868–11873, 2006.
- [31] S. Grimbs, J. Selbig, S. Bulik, H. Holzhütter, and R. Steuer. The stability and robustness of metabolic states: identifying stabilizing sites in metabolic networks. *Molecular Systems Biology*, 3:146, 2007.

- [32] W. Liebermeister, U. Baur, and E. Klipp. Biochemical network models simplified by balanced truncation. *FEBS Journal*, 272(16):4034 – 4043, 2005.
- [33] R. Heinrich and S. Schuster. *The Regulation of Cellular Systems*. Chapman & Hall, 1996.
- [34] J.-H.S. Hofmeyr. Metabolic control analysis in a nutshell. In *ICSB 2001 Online Proceedings*, <http://www.icsb2001.org/toc.html>, 2001.
- [35] E. Klipp and R. Heinrich. Competition for enzymes in metabolic pathways: implications for optimal distributions of enzyme concentrations and for the distribution of flux control. *BioSystems*, 54:1–14, 1999.
- [36] T. Höfer and R. Heinrich. A second-order approach to metabolic control analysis. *J. Theor. Biol.*, 164:85–102, 1993.
- [37] W. Liebermeister, E. Klipp, S. Schuster, and R. Heinrich. A theory of optimal differential gene expression. *BioSystems*, 76:261–278, 2004.
- [38] B.P. Ingalls. A frequency domain approach to sensitivity analysis of biochemical systems. *J Phys Chem B*, 108:1143–1152, 2004.
- [39] W. Liebermeister. Response to temporal parameter fluctuations in biochemical networks. *J. Theor. Biol.*, 234(3):423–438, 2005.
- [40] C. Gille, C. Bölling, A. Hoppe, S. Bulik, S. Hoffmann, K. Hübner, A. Karlstädt, R. Ganeshan, M. König, K. Rother, M. Weidlich, J. Behre, and H. Holzhütter. HepatoNet1: a comprehensive metabolic reconstruction of the human hepatocyte for the analysis of liver physiology. *Molecular Systems Biology*, 6:411, 2010.
- [41] C. Chassagnole, B. Rais, E. Quentin, D. A. Fell, and J. Mazat. An integrated study of threonine-pathway enzyme kinetics in *Escherichia coli*. *Biochem J*, 356:415–423, 2001.
- [42] M. König and H.G. Holzhütter. Kinetic modeling of human hepatic glucose metabolism in T2DM predicts higher risk of hypoglycemic events in rigorous insulin therapy. *J Biol Chem.*, 287:36978–36989, 2012.
- [43] B. Teusink, M.C. Walsh, K. van Dam, and H.V. Westerhoff. The danger of metabolic pathways with turbo design. *Trends Biochem Sci*, 23:162–169, 1998.
- [44] D. Segrè, A. DeLuna, G. M. Church, and R. Kishony. Modular epistasis in yeast metabolism. *Nature Genetics*, 37:77 – 83, 2005.
- [45] M. Costanzo et al. The genetic landscape of a cell. *Science*, 327(5964):425–431, 2010.
- [46] D.T. Gillespie. The chemical Langevin equation. *J. Chem. Phys.*, 113(1):297–306, 2000.
- [47] A.H.Y. Tong, G. Lesage, G. Bader, H. Ding, H. Xu, X. Xin, J. Young et al., C. G. Burd, S. Munro, C. Sander, J. Rine, J. Greenblatt, M. Peter, A. Bretscher, G. Bell, F. P. Roth, G. Brown, B. Andrews, H. Bussey, and C. Boone. Global mapping of the yeast genetic interaction network. *Science*, 303:808–813, 2004.

- [48] R. Steuer, J. Kurths, O. Fiehn, and W. Weckwerth. Observing and interpreting correlations in metabolomics networks. *Bioinformatics*, 19(8):1019–1026, 2003.
- [49] R. Heinrich and S. Schuster. *The Regulation of Cellular Systems*. Chapman & Hall, 1996.
- [50] A. Bar-Even, E. Noor, Y. Savir, W. Liebermeister, D. Davidi, D.S. Tawfik, and R. Milo. The moderately efficient enzyme: evolutionary and physicochemical trends shaping enzyme parameters. *Biochemistry*, 21:4402–4410, 2011.
- [51] R. N. Goldberg. Thermodynamics of enzyme-catalyzed reactions: Part 6 - 1999 update. *J Phys Chem Ref Data*, 28:931, 1999.
- [52] I. Schomburg, A. Chang, C. Ebeling, M. Gremse, C. Heldt, G. Huhn, and D. Schomburg. BRENDA, the enzyme database: updates and major new developments. *Nucleic Acids Research*, 32:Database issue:D431–433, 2004.
- [53] W. Liebermeister. Predicting physiological concentrations of metabolites from their molecular structure. *J. Comp. Biol.*, 12(10):1307–1315, 2005.
- [54] T. Lubitz, M. Schulz, E. Klipp, and W. Liebermeister. Parameter balancing for kinetic models of cell metabolism. *J. Phys. Chem. B*, 114(49):16298–16303, 2010.
- [55] M. Ederer and E.D. Gilles. Thermodynamically feasible kinetic models of reaction networks. *Biophys. J.*, 92:1846–1857, 2007.
- [56] R. Wegscheider. Über simultane Gleichgewichte und die Beziehungen zwischen Thermodynamik und Reaktionskinetik homogener Systeme. *Z. Phys. Chem.*, 39:257–303, 1902.
- [57] S. Schuster and R. Schuster. A generalization of Wegscheider’s condition. Implications for properties of steady states and for quasi-steady-state approximation. *J. Math. Chem.*, 3:25–42, 1989.
- [58] C. Reder. Metabolic control theory: a structural approach. *J. Theor. Biol.*, 135:175–201, 1988.
- [59] J.B.S. Haldane. *Enzymes*. Longmans, Green and Co., London. (republished in 1965 by MIT Press, Cambridge, MA), 1930.
- [60] D.A. Beard, E. Babson, E. Curtis, and H. Qian. Thermodynamic constraints for biochemical networks. *J. Theor. Biol.*, 228(3):327–333, 2004.
- [61] Brett W. Bader, Tamara G. Kolda, et al. Matlab tensor toolbox version 2.5. Available online, January 2012.
- [62] Brett W. Bader and Tamara G. Kolda. Efficient MATLAB computations with sparse and factored tensors. *SIAM Journal on Scientific Computing*, 30(1):205–231, December 2007.
- [63] S. Bulik, S. Grimbs, C. Huthmacher, J. Selbig, and H. Holzhütter. Kinetic hybrid models composed of mechanistic and simplified enzymatic rate laws: A promising method for speeding up the kinetic modelling of complex metabolic networks. *FEBS Journal*, 276:410, 2009.
- [64] E.T. Jaynes. Information theory and statistical mechanics. *Physical Review*, 106:620–630, 1957.

- [65] R. Chait, A. Craney, and R. Kishony. Antibiotic interactions that select against resistance. *Nature*, pages 668–671, 2007.
- [66] M. Pellegrini, E.M. Marcotte, M.J. Thompson, D. Eisenberg, and T.O. Yeates. Assigning protein functions by comparative genome analysis: Protein phylogenetic profiles. *Proc Natl Acad Sci USA*, 96(8):4285–4288, 1999.
- [67] Y. Benjamini and Y. Hochberg. Controlling the false discovery rate: a practical and powerful approach to multiple testing. *Journal of the Royal Statistical Society, Series B* 57(1):289–300, 1995.

A Mathematical symbols

Network	
Internal metabolite levels	c_i
External metabolite levels	x_j
Enzyme levels	u_l
Stoichiometric matrix (all metabolites)	\mathbf{N}
Stoichiometric matrix (internal metabolites)	\mathbf{N}^{int}
Stoichiometric matrix (external metabolites)	\mathbf{N}^{ext}
Cooperativity coefficients	h_l
Stoichiometric coefficients	n_{il} (signed) or m_{li}^{\pm} (absolute)
Allosteric activation arrows	m_{li}^A
Allosteric inhibition arrows	m_{li}^I
Rate laws and rate constants	
Rate laws	$r(\mathbf{c}, \mathbf{u}, \mathbf{x}) = u_l r_l^f(\mathbf{c}, \mathbf{x})$
Michaelis-Menten constants	k_{li}^M
Activation constants	k_{li}^A
Inhibition constants	k_{li}^I
Catalytic constants	k_l^{\pm}
Maximal velocities	$v_l^{\text{max}\pm} = u_l k_l^{\pm}$
Velocity constants	$k_l^V = \sqrt{k_l^+ k_l^-}$
Steady state	
Mass-action ratios	$q_l^{\text{ma}} = \prod_i c_i^{n_{il}}$
Equilibrium constants	$k_l^{\text{eq}} = \prod_i (c_i^{\text{eq}})^{n_{il}}$
Standard chemical potentials	$\mu_i^{(0)}$
Chemical potentials	$\mu_i = \mu_i^{(0)} + RT \ln c_i$
driving forces	$A_l = -\Delta\mu_l$
Microscopic flux ratio ζ_l	$\zeta_l = v_l^+ / v_l^- = e^{h_l A_l / RT}$
Elasticity sampling	
Saturation values	$\beta_{li}^M, \beta_{li}^A, \beta_{li}^I$
Unscaled elasticities	$\bar{E}_{c_i}^{v_l} = \frac{\partial r_l}{\partial c_i}$
Scaled elasticities	$E_{c_i}^{v_l} = \frac{\partial \ln r_l }{\partial \ln c_i}$
Metabolic control analysis	
Stationary fluxes	$v_l = j(\mathbf{u}, \mathbf{x})$
Stationary concentrations	$c_i = s_i(\mathbf{u}, \mathbf{x})$
Jacobian matrix	\mathbf{J}
Unscaled response coefficients	$\bar{R}_{u_l}^{s_i} = \frac{\partial s_i}{\partial u_l}, \bar{R}_{u_l}^{j_j} = \frac{\partial j_j}{\partial u_l}$
Unscaled control coefficients	$\bar{C}_{v_l}^{s_i} = \bar{R}_{u_l}^{s_i} / \bar{E}_{u_l}^{v_l}, \bar{C}_{v_l}^{j_j} = \bar{R}_{u_l}^{j_j} / \bar{E}_{u_l}^{v_l}$
Scaled response/control coefficients	$R_{u_l}^{s_i} = C_{v_l}^{s_i} = \frac{\partial \ln s_i}{\partial \ln u_l}, R_{u_l}^{j_j} = C_{v_l}^{j_j} = \frac{\partial \ln j_j }{\partial \ln u_l}$

Table 1: Symbols used in the article. Network elements are denoted by i (metabolites) and l (reactions). Second-order elasticities, response coefficients, and control coefficients are defined accordingly.

B Mathematical formalism for kinetic models

Metabolic networks and kinetic models A metabolic network model is defined by its reaction stoichiometries and by arrows for allosteric activation and inhibition (Figure 8 (a)). For convenience, the stoichiometric coefficients n_{li} between metabolite i and enzyme l , multiplied by the reaction's cooperativity coefficient h_l , are denoted by molecularities m_{li}^+ (for substrates) and m_{li}^- (for products) (i.e., $h_l n_{li} = m_{li}^+ - m_{li}^-$) as in [19]. The stoichiometric coefficients and the allosteric regulation coefficients m_{li}^A and m_{li}^I (activation: $m_{li}^A = 1$; inhibition: $m_{li}^I = 1$; zero values otherwise) form the structure matrices. In kinetic models [33], reaction rates are determined by rate laws $r_l(\mathbf{c}, \mathbf{u}, \mathbf{x}) = u_l r'_l(\mathbf{c}, \mathbf{x})$ and their rate constants (Figure 8 (b)). The modular rate laws [19] contain two types of rate constants: reactant constants k^M for reactants, activation constants k^A for activators, and inhibition constants k^I for inhibitors (in mM) describe how strongly molecules bind to the enzyme; formally, they are dissociation constants. The catalytic constants k^\pm (in s^{-1}) describe the speed of the forward and reverse rates, and their ratios are fixed by Haldane relations. Given stoichiometric matrix and rate laws, the internal metabolite concentrations c_i follow the system equations $dc_i/dt = \frac{1}{V_i} \sum_l n_{il} r_l(\mathbf{c}, \mathbf{u}, \mathbf{x})$, in which external metabolite levels x_j and enzyme levels u_l appear as parameters. We assume that metabolite i is homogeneously distributed in a compartment of constant size V_i . Metabolite concentrations are given in $\text{mM} = \text{mol}/\text{m}^3$, reaction rates as amounts per time (mol/s), enzyme levels as amounts (mol), and volumes in m^3 . In single-compartment models, we may formally set the compartment size to 1 (dimensionless) and measure the rates in mM/s and enzyme levels in mM . As long as models are only analysed in terms of steady states, flux units can be chosen arbitrarily.

Thermodynamic quantities Steady states and kinetic of metabolic systems are influenced by thermodynamics. We consider a metabolic system with metabolite concentrations s_i , reaction rates v_l , equilibrium constants k_l^{eq} , and chemical potentials μ_i . The chemical potentials μ_i are the derivatives $\mu_i = \partial G / \partial n_i$ of the Gibbs free energy with respect to the metabolites' mole numbers n_i . For ideal mixtures (small amounts of metabolites in aqueous solution, no mixture effects, activity coefficients of 1), they can be computed by the formula¹

$$\mu_i = \mu_i^{(0)} + RT \ln c_i / c_{\text{std}} \quad (6)$$

with Boltzmann gas constant R , absolute temperature T , and the chemical potential $\mu_i^{(0)}$ of the i^{th} metabolite at standard concentration c_{std} (usually chosen to be 1 mM). In the following, we shall omit the division by c_{Σ} , assuming that all concentrations are measured in units of the standard concentration. The ratio $q_l^{\text{ma}} = \prod_i (c_i)^{n_{il}}$ of product and substrate levels for a reaction is called the mass-action ratio. A reaction shows the same mass-action ratio $k_l^{\text{eq}} = \prod_i (c_i^{\text{eq}})^{n_{il}}$, in all chemical equilibrium states. This ratio, called equilibrium constant k_l^{eq} , can also be written as $k^{\text{eq}} = -\Delta\mu^{(0)}$. The driving force A_r is defined as the negative change of chemical potentials (in kJ/mol) associated with a reaction event in some, possibly

¹ The thermodynamic-kinetic formalism [55] defines a quantity related to the chemical potential, the thermokinetic potential $\xi_i = e^{\mu_i/RT}$. It can be formally split into $\xi_i = C_i c_i$, where C_i is called the capacity. For ideal mixtures (satisfying Eq. (6)), the formula reads $\xi_i = e^{\mu_i^{(0)}/RT} c_i$ with a capacity $C_i = e^{\mu_i^{(0)}/RT}$.

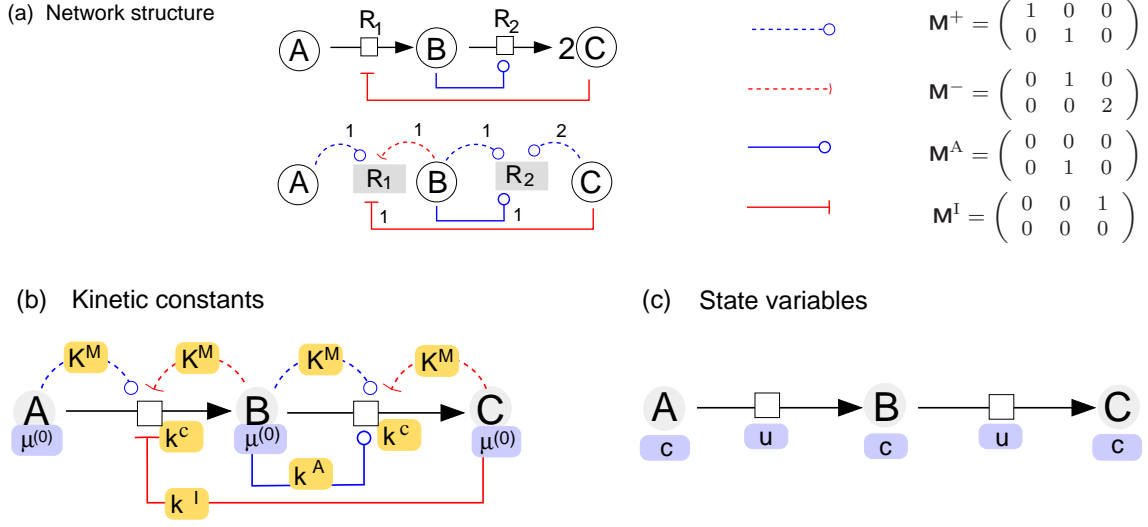


Figure 8: **Elements of kinetic metabolic models.** (a) Metabolic network and structure matrices. The metabolic pathway in the example consists of two reactions $A \rightleftharpoons B$ and $B \rightleftharpoons 2C$. Reaction R_1 is inhibited by the product C , while reaction R_2 is activated by its own substrate B . Below, the same pathway is shown as a bipartite network. Each arrow carries a number: dotted arrows show stoichiometric coefficients for substrates and products, regulation arrows (solid) carry values of 1. Right: the arrows can be represented by structure matrices \mathbf{M}^+ , \mathbf{M}^- , \mathbf{M}^A , and \mathbf{M}^I whose rows and columns correspond to reactions and metabolites. (b) rate constants in modular rate law. Standard chemical potentials $\mu_i^{(0)}$ of the metabolites determine the equilibrium constants. Dissociation constants k_{li}^M , k_{li}^A , or k_{li}^I are assigned to all stoichiometry or regulation arrows, while velocity constants k_{li}^V are assigned to reactions. Together, these constants determine the catalytic constants k_{li}^\pm . (c) A metabolic state is characterised by metabolite levels c_i and enzyme levels u_i .

non-steady, metabolic state.

$$A_l = -\Delta\mu_l = -\sum_i \mu_i n_{il}. \quad (7)$$

With the equilibrium constant k_l^{eq} and the mass-action ratio q_l^{ma} for reaction l , it reads

$$A_l = -\sum_i n_{il} \mu_i = RT \ln k_l^{\text{eq}} / q_l^{\text{ma}}. \quad (8)$$

In generalised Michaelis-Menten rate laws, the ratio of forward and backward rates v_l^\pm of reaction l can be expressed as

$$\zeta_l = v_l^+ / v_l^- = e^{h_l A_l / RT} = k_l^{\text{eq}} / \prod c_i^{n_i}. \quad (9)$$

The laws of thermodynamics impose three sorts of constraints on kinetic models: common signs of fluxes and driving forces, Wegscheider conditions, and Haldane relations. As spontaneous thermodynamical processes, chemical reactions must produce a positive entropy per volume $\sigma = v_l A_l / T$. This entails that

any (non-zero) reaction rate v_l must have the same sign as the driving force A_l . The condition [56, 57] $\mathbf{K}^\top \ln \mathbf{k}^{\text{eq}} = 0$ have to be satisfied for the vector $\ln \mathbf{k}^{\text{eq}}$ of logarithmic equilibrium constants, where K is a null space matrix satisfying $NK = 0$. Similar Wegscheider conditions hold for any quantities that can be written, in vectorial form, as $\mathbf{x} = \mathbf{N}\mathbf{y}$, such as the logarithmic mass-action ratios $\ln q_i^{\text{ma}}$ and the driving forces A_l . The fact that reaction rates $v_l(\mathbf{c}^{\text{eq}}, \mathbf{u})$ vanish at chemical equilibrium implies a Haldane relation [24, 55] between equilibrium constant and rate constants. For modular rate laws, it reads

$$k_l^{\text{eq}} = k_l^+ / k_l^- \prod_i (k_{i_i}^{\text{M}})^{n_{ii}}. \quad (10)$$

To satisfy it, we define the turnover constant k_l^{V} for reaction l by $k_l^{\text{V}} = \sqrt{k_l^+ k_l^-}$, combine this formula with Eq. (10), and obtain a formula for the turnover rates.

The modular rate laws The modular rate laws are standardised reversible rate laws that capture all reaction stoichiometries, several enzyme mechanisms, and various types of allosteric regulation. Formulae for all rate laws and their elasticities are given in the supplementary material of [19]. As an example, consider a reaction $A + B \rightleftharpoons 2C$ without allosteric effectors. The common modular (CM) rate law, a generalised form of the reversible Michaelis-Menten kinetics, reads

$$r(a, b, c, u) = u \frac{k^+ (a/k_{\text{A}}^{\text{M}})(b/k_{\text{B}}^{\text{M}}) - k^- (c/k_{\text{C}}^{\text{M}})^2}{(1 + a/k_{\text{A}}^{\text{M}})(1 + b/k_{\text{B}}^{\text{M}}) + (1 + c/k_{\text{C}}^{\text{M}})^2 - 1} \quad (11)$$

with reactant constants k_{A}^{M} , k_{B}^{M} , and k_{C}^{M} (in mM) and catalytic constants k^+ and k^- (in s^{-1}) for the forward and reverse directions. Substrates and products bind rapidly, independently, and in random order. Physically, the reactant constants $k_{i_i}^{\text{M}}$ are dissociation constants of the elementary binding steps. Like the K_{M} values in Michaelis-Menten kinetics, they represent reactant concentrations that would lead to half-maximal saturation (or $1/|n_{ii}|$ -maximal saturation if $|n_{ii}| > 1$). The catalytic constants $k^{\text{cat}\pm}$, in contrast, are the rate constants of the slow conversion between substrates and products.

Depending on the case, modular rate laws can further be modified: if the enzyme is regulated by allosteric effector molecules, this can be described, for instance, by prefactors $\beta_{\text{X}}^{\text{A}} = \frac{x/k_{\text{X}}^{\text{A}}}{1+x/k_{\text{X}}^{\text{A}}}$ for activators X or $\alpha_{\text{Y}}^{\text{I}} = \frac{1}{1+y/k_{\text{Y}}^{\text{I}}}$ for inhibitors Y. Moreover, the rate laws can be turned into a sigmoid kinetics by choosing a Hill-like exponent h . Finally, there are other types of rate law with the same parameters, but other denominators, for instance, the saturable modular (SM) rate law

$$r(a, b, c, u) = u \frac{k^+ (a/k_{\text{A}}^{\text{M}})(b/k_{\text{B}}^{\text{M}}) - k^- (c/k_{\text{C}}^{\text{M}})^2}{(1 + a/k_{\text{A}}^{\text{M}})(1 + b/k_{\text{B}}^{\text{M}})(1 + c/k_{\text{C}}^{\text{M}})^2}. \quad (12)$$

In the denominator, the terms for all substrates and products are simply multiplied. In all modular rate laws, the rate constants need to satisfy Haldane relations. This can be ensured by using predetermined equilibrium constants treating the velocity constants $k_l^{\text{V}} = \sqrt{k_l^+ k_l^-}$, the geometric mean of forward and reverse catalytic constants, as a free parameter. The individual catalytic constants k_l^+ and k_l^- are then

given by

$$k_l^\pm = k_l^V (k_l^{\text{eq}} \prod_i (k_{li}^M)^{-n_{il}})^{\pm 1/2} \quad (13)$$

will satisfy the Haldane relations.

Metabolic control analysis Steady states are states in which all variables – in particular, the metabolite levels – remain constant in time. The steady-state fluxes $j_l(\mathbf{u}, \mathbf{x})$ and concentrations $s_i(\mathbf{u}, \mathbf{x})$ depend on the enzyme levels u_l and external metabolite levels x_j , but the dependence is usually complicated and not explicitly known (see Figure 8 (c)). However, if a steady state is given, its sensitivities to parameter changes can be computed easily from the elasticities. The response coefficients $R_{p_m}^y = \partial y / \partial p_m$ are the sensitivities of an output variable y – e.g., a stationary concentration s_i or a flux j_l – to model parameters p_m . Using a set of reaction-specific parameters p_l – for instance enzyme levels u_l – we can scale the response coefficients $\bar{R}_{v_l}^y$ by the elasticities $\bar{E}_{p_l}^{v_l}$ and obtain the control coefficients $\bar{C}_{v_l}^y = \bar{R}_{p_l}^y / \bar{E}_{p_l}^{v_l}$ (Figure 1 (c)). The control coefficients describe how perturbations spread from a perturbed reaction, no matter which parameter caused the initial perturbation. Thus, response coefficients refer to perturbed parameters and control coefficients to perturbed reactions. Parameters like the dilution rate or the temperature can affect many reactions, and their effects are described by response coefficients $\bar{R}_{p_m}^y = \sum_l \bar{C}_{v_l}^y \bar{E}_{p_m}^{v_l}$ (for more details, see SI I.2 and [58, 36, 34]). Elasticities, response coefficients, and control coefficients exist in unscaled form $\partial y / \partial x$ and in the scaled form $\partial \ln y / \partial \ln x$ (see SI C). If an enzyme catalyses a single reaction and if the enzyme level appears as a prefactor in the rate law, its scaled response and control coefficients are identical. The summation and connectivity theorems [33], a central result of MCA, establish linear dependencies among the control coefficients along a stationary flux mode or in the reactions surrounding a common metabolite. Quantities and formulae related to fluctuations in time (such as spectral response coefficients, spectral power density, and variability on different time scales) are described in the SI.

Synergies between enzyme perturbations Synergistic effects of enzyme pairs on a flux v (or on other steady-state variables) can be approximated by the second-order response coefficients. Assume that two enzyme levels u_a and u_b are decreased to values u_a^* and u_b^* , leading to relative flux changes $w_a = v^a / v$, $w_b = v^b / v$ for the single inhibitions and $w_{ab} = v^{ab} / v$ for the double inhibition. To compare these numbers, we define the synergistic effect

$$\eta_{ab}^v = \ln \frac{w_{ab}}{w_a w_b}. \quad (14)$$

Positive values of η_{ab}^v indicate buffering synergy ($w_{ab} > w_a w_b$), negative values aggravating synergy ($w_{ab} < w_a w_b$). If $w_{ab} = w_a w_b$, there is no synergy. In a second-order expansion around the unperturbed state, the synergistic effect can be approximated by (see SI I.4)

$$\eta_{ab}^v \approx R_{u_a u_b}^y \Delta \ln u_a \cdot \Delta \ln u_b, \quad (15)$$

so the scaled response coefficients $R_{u_a u_b}^y$ measure the synergy strength between two enzymes. If perturbations and output variables are measured on non-logarithmic scale, the synergistic effects $\bar{\eta}_{ab}^v = w_{ab} - w_a - w_b$ can be approximated by $\bar{\eta}^v \approx \bar{R}_{u_a u_b}^y \Delta u_a \Delta u_b$ with the unscaled response coefficient $\bar{R}_{u_a u_b}^y$.

C Reaction elasticities and their dependencies

Scaled and unscaled reaction elasticities Given a rate law $r_l(u_l, \mathbf{c})$, the reaction elasticities are defined by partial derivatives (“unscaled elasticities”)

$$\bar{E}_{c_i}^{v_l} = \frac{\partial r_l}{\partial c_i}, \quad \bar{E}_{c_i c_j}^{v_l} = \frac{\partial^2 r_l}{\partial c_i \partial c_j} \quad (16)$$

or by logarithmic partial derivatives (“scaled elasticities”)

$$E_{c_i}^{v_l} = \frac{\partial \ln |r_l|}{\partial \ln c_i}, \quad E_{c_i c_j}^{v_l} = \frac{\partial^2 \ln |r_l|}{\partial \ln c_i \partial \ln c_j}. \quad (17)$$

Scaled elasticities are dimensionless and can be seen as effective reaction orders: for mass-action kinetics, they are nothing but the substrate molecularities; for enzymatic reactions in full saturation, they vanish. Scaled and unscaled elasticities can be interconverted by

$$E_{c_i}^{v_l} = \frac{c_i}{v_l} \bar{E}_{c_i}^{v_l}, \quad E_{c_i c_j}^{v_l} = \frac{c_i c_j}{v_l} \bar{E}_{c_i c_j}^{v_l} - \frac{c_i c_j}{v_l^2} \bar{E}_{c_i}^{v_l} \bar{E}_{c_j}^{v_l} + \delta_{ij} \frac{c_i}{v_l} \bar{E}_{c_i}^{v_l} \quad (18)$$

$$\bar{E}_{c_i}^{v_l} = \frac{v_l}{c_i} E_{c_i}^{v_l}, \quad \bar{E}_{c_i c_j}^{v_l} = \frac{v_l}{c_i c_j} \left[E_{c_i c_j}^{v_l} + E_{c_i}^{v_l} E_{c_j}^{v_l} - \delta_{ij} E_{c_i}^{v_l} \right]. \quad (19)$$

Analogous formulae hold for all kinds of sensitivities, in particular enzyme elasticities, control coefficients, and response coefficients [58, 34].

Elasticities and thermodynamic force The derivatives of kinetic laws with respect to enzyme concentrations u_p , metabolite concentrations c_j , or other arguments of the rate law $r_l(\cdot)$ are called reaction elasticities (see Figure 1 (a)). Derivatives $\bar{E}_{c_i}^{v_l} = \partial r_l / \partial c_i$ and $\bar{E}_{c_i c_j}^{v_l} = \partial^2 r_l / (\partial c_i \partial c_j)$ are called unscaled metabolite elasticities. The derivatives $E_{c_i}^{v_l} = \frac{\partial \ln |r_l|}{\partial \ln c_i}$ and $E_{c_i c_j}^{v_l} = \frac{\partial^2 \ln |r_l|}{\partial \ln c_i \partial \ln c_j}$ on logarithmic scale, called scaled elasticities, describe relative changes. Elasticities depend on the rate laws, but are partially determined by thermodynamics. In reversible rate laws, the net reaction rate $v_l = v_l^+ - v_l^-$ is the difference of forward and reverse rates, whose ratio $v_l^+ / v_l^- = e^{A_l / RT}$ is determined by the driving force A_l (in kJ/mol). The driving force, in turn follows from the reactant concentrations and the equilibrium constant as $A_l = -\Delta G_l = RT \ln \frac{k^{\text{eq}}}{\prod_i c_i^{n_i}}$ (see Figure 1 (b)). The driving force can be seen as a thermodynamic driving force: if it is large, the forward flux dominates and the net rate becomes sensitive to substrate fluctuations, but less sensitive to product fluctuations; therefore, the substrate elasticity increases and the product elasticity decreases. Close to chemical equilibrium, at driving forces close to zero, the scaled elasticities diverge.

Independently sampled elasticities would yield inconsistent models A main problem with SKM is that the elasticities are sampled independently, which implies that the corresponding kinetic models may violate some important constraints. If forward and reverse rates in kinetic models were described by independent reactions, this would be justified: the sampled elasticities could be directly translated into rate constants, and each sampled elasticity matrix would define a specific kinetic model. However, for reversible rate laws, independent elasticity sampling leads to inconsistent results. For instance, consider

a reaction $A \rightleftharpoons B$ with reversible mass-action kinetics $v = k^+ a - k^- b$: the scaled reaction elasticities read $E_A = k^+ a/v$ (for substrate A) and $E_B = k^- b/v$ (for product B), so their difference $E_A - E_B = 1$ is fixed. If we sample both elasticities independently, this relationship is violated and our sampled values cannot be realised by reversible mass-action rate laws. Similar constraints hold for any thermodynamically consistent reversible rate laws.

The inconsistency can also be shown by looking at thermodynamic constraints. Consider a toy example: the reaction $A \rightarrow B$ is catalysed by two isoenzymes with reversible mass-action kinetics:

$$\begin{aligned} v_1 &= r_1(a, b) = k_1^+ a - k_1^- b \\ v_2 &= r_2(a, b) = k_2^+ a - k_2^- b. \end{aligned} \quad (20)$$

The symbols a and b denote the concentrations of A and B, and k_1^\pm and k_2^\pm the rate constants. In each reaction, the ratio between forward and backward rate constant must yield the same equilibrium constant:

$$k^{\text{eq}} = \frac{k_1^+}{k_1^-} = \frac{k_2^+}{k_2^-}. \quad (21)$$

Therefore, the scaled elasticity matrix reads

$$E = \begin{pmatrix} \frac{\partial \ln r_1}{\partial \ln a} & \frac{\partial \ln r_1}{\partial \ln b} \\ \frac{\partial \ln r_2}{\partial \ln a} & \frac{\partial \ln r_2}{\partial \ln b} \end{pmatrix} = \begin{pmatrix} k_1^+ \frac{a}{v_1} & -k_1^- \frac{b}{v_1} \\ k_2^+ \frac{a}{v_2} & -k_2^- \frac{b}{v_2} \end{pmatrix} = \begin{pmatrix} \frac{k^{\text{eq}} a}{k^{\text{eq}} a - b} & \frac{-b}{k^{\text{eq}} a - b} \\ \frac{k^{\text{eq}} a}{k^{\text{eq}} a - b} & \frac{-b}{k^{\text{eq}} a - b} \end{pmatrix} = \begin{pmatrix} \frac{\zeta}{\zeta - 1} & \frac{-1}{\zeta - 1} \\ \frac{\zeta}{\zeta - 1} & \frac{-1}{\zeta - 1} \end{pmatrix} \quad (22)$$

with $\zeta = k^{\text{eq}}/(b/a)$. All four elasticities are determined by the same parameter ζ , so sampling them independently would lead to contradictions.

Elasticities of the modular rate laws The scaled metabolite elasticities of the SM rate law Eq. (12) contain the thermodynamic term and four terms corresponding to the influences of substrates, products, activators, and inhibitors:

$$E_{c_i}^{v_i} = \frac{\zeta_i m_{i_i}^+ - m_{i_i}^-}{\zeta_i - 1} - m_{i_i}^+ \alpha_{i_i}^M - m_{i_i}^- \beta_{i_i}^M + m_{i_i}^A \alpha_{i_i}^A - m_{i_i}^I \beta_{i_i}^I \quad (23)$$

For reactions close to equilibrium (small A_i), or almost irreversible forward reactions ($|A_i| \rightarrow \infty$), the first three terms can be approximated by

$$\begin{aligned} |A_i| \approx 0 &: \frac{RT}{A_i} (m_{i_i}^+ - m_{i_i}^-) + m_{i_i}^+ \alpha_{i_i}^M - m_{i_i}^- \beta_{i_i}^M \\ A_i \rightarrow \infty &: (m_{i_i}^+ - m_{i_i}^-) e^{-A_i/RT} + m_{i_i}^+ \alpha_{i_i}^M - m_{i_i}^- \beta_{i_i}^M \\ A_i \rightarrow -\infty &: (m_{i_i}^- - m_{i_i}^+) e^{-|A_i|/RT} - m_{i_i}^+ \beta_{i_i}^M + m_{i_i}^- \alpha_{i_i}^M. \end{aligned} \quad (24)$$

The last two terms in these formulae correspond to the sampling rule of structural kinetic modelling [30], while the first term adds a thermodynamic correction. The scaled elasticities for the common modular rate

law read

$$E_{c_j}^{v_l} = \beta_{lj} \frac{\zeta_l m_{lj}^+ - m_{lj}^-}{\zeta_l - 1} - \beta_{lj} \frac{m_{lj}^+ \psi_l^+ + m_{lj}^- \psi_l^-}{\psi_l^+ + \psi_l^- - 1} + m_{li}^A \alpha_{li}^A - m_{li}^I \beta_{li}^I. \quad (25)$$

Formulae for second-order elasticities, unscaled elasticities, parameter elasticities, and other types of modular rate laws are given in [19].

Independently sampled saturation values yield consistent models Elasticity sampling as proposed here is justified by the fact that, given consistent fluxes and driving forces, any choice of the saturation values will correspond to a consistent kinetic model and vice versa. This can be proven as follows. Consider a kinetic model with modular rate laws and a thermodynamically consistent flux distribution \mathbf{v} . For simplicity, enzyme levels are subsumed in the catalytic constants k_l^\pm . As shown in [19], a consistent set of parameters, realising \mathbf{v} , could be obtained by the following model construction procedure:

1. Freely choose standard chemical potentials $\mu_i^{(0)}$ and determine the equilibrium constants.
2. Determine concentrations c_i such that the signs of driving forces and fluxes agree.
3. Freely choose Michaelis constants k_{li}^M and activation and inhibition constants k_{li}^A and k_{li}^I .
4. Set all velocity constants to preliminary values $k_l^{V'}$. Compute the catalytic constants $k_l^{\pm'}$ from the Haldane relations. Compute the reaction rates v_l' from the rate laws. By construction (due to the thermodynamic flux constraints and the thermodynamically feasible rate laws), these rates will have the same signs as the predefined fluxes. Therefore, we can set the actual velocity constants to $k_l^V = (v_l/v_l') k_l^{V'}$, which leads to the correct reaction rates v_l .
5. If our flux distribution contains inactive reactions, we can decide, for each of them, whether we assume a vanishing thermodynamic force, a vanishing velocity constant, or a vanishing enzyme level. In the first case, we need to apply the strict energetic feasibility criterion for this reaction (i.e., require that the driving force vanishes); in the other cases, there is no feasibility criterion for the reaction, and the k^V value or enzyme level is set to zero.

If this procedure yields correct models, this will also hold for elasticity sampling. In elasticity sampling, we first determine consistent fluxes v_l and driving forces A_l that can be realised by a choice of standard chemical potentials $\mu_i^{(0)}$ and concentrations c_i . If now we choose the saturation constants, any choice is equivalent to a choice of k_{li}^M , k_{li}^A , and k_{li}^I in the algorithm above. Thus, the quantities chosen until this point correspond exactly to the results of step 3. Thus, steps 4 and 5 will yield a unique, consistent set of parameters. Therefore, models obtained by elasticity sampling satisfy all relevant constraints.

Dependence between first- and second-order elasticities For a given modular rate law, the scaled elasticities can be computed from the stoichiometric coefficients, driving forces, and saturation values. This dependence on common factors leads to constraints between the elasticities, and as these factors are varied, the varying elasticities will be statistically dependent. Here is an example. Whenever a driving force becomes large, the substrate elasticities will become larger and the product elasticities will become smaller. When comparing all elasticities in a network, or when comparing the different instances of an ensemble

model, this relationship between driving force and elasticities leads to positive correlations among substrate elasticities, positive correlations among product elasticities, and negative correlations between substrate and product elasticities. On the contrary, all all unscaled elasticities in a pathway tend to rise with the pathway flux, leading to positive correlations between them (when comparing model instances with different flux distributions). Just like first-order elasticities are dependent, second-order elasticities will be dependent on them. This entails statistical dependencies, both between different sampled versions of a model (e.g., assuming different values of the driving forces) and between the reactions in a single model. Second-order elasticities $E_{c_i c_j}^{v_l}$ will tend to be negatively correlated to the corresponding product $E_{c_i}^{v_l} E_{c_j}^{v_l}$ of first-order elasticities. To see this, consider a simple mass-action or power-law rate law without allosteric regulation: the elasticities are directly given by the thermodynamic terms

$$E_{c_i}^{v_l} = \frac{m_{l_i}^+ \zeta_l - m_{l_i}^-}{\zeta_l - 1} = \begin{cases} i \text{ is a substrate} & : \frac{\zeta_l}{\zeta_l - 1} m_{l_i}^+ \\ i \text{ is a product} & : \frac{-1}{\zeta_l - 1} m_{l_i}^- \end{cases} \quad (26)$$

$$E_{c_i c_j}^{v_l} = -\frac{\zeta_l h_l^2 n_{il} n_{jl}}{(\zeta_l - 1)^2} = \begin{cases} i, j \text{ are substrates} & : -\frac{\zeta_l m_{l_i}^+ m_{l_j}^+}{(\zeta_l - 1)^2} \approx -\frac{1}{\zeta} E_{c_i}^{v_l} E_{c_j}^{v_l} \\ \text{one substrate, one product} & : \frac{\zeta_l m_{l_i}^+ m_{l_j}^-}{(\zeta_l - 1)^2} \approx -E_{c_i}^{v_l} E_{c_j}^{v_l} \\ i, j \text{ are products} & : -\frac{\zeta_l m_{l_i}^- m_{l_j}^-}{(\zeta_l - 1)^2} \approx -\zeta E_{c_i}^{v_l} E_{c_j}^{v_l} \end{cases} \quad (27)$$

In the formula, reactants are classified as substrates and products according to the nominal reaction formula, not according to the actual flux direction; the flux direction enters the formulae via ζ_l , whose being larger or smaller than 1 depends on the sign of the driving force and thus on the flux direction. The second-order elasticities can formally be written as

$$E_{c_i c_j}^{v_l} = \vartheta_{ij}^l E_{c_i}^{v_l} E_{c_j}^{v_l} \quad (28)$$

where, in the present case (non-regulated mass-action rate law), the prefactor ϑ_{ij}^l reads

$$\vartheta_{ij}^l = \begin{cases} i, j \text{ are substrates} & : -1/\zeta_l \\ \text{one substrate, one product} & : -1 \\ i, j \text{ are products} & : -\zeta_l \end{cases} \quad (29)$$

Due to its negative values, we can expect a negative statistical correlation between the second-order elasticity $E_{c_i c_j}^{v_l}$ and the product $E_{c_i}^{v_l} E_{c_j}^{v_l}$ of first-order elasticities. In particular, close to equilibrium (where $A_l \approx 0$ and therefore $\zeta_l \approx 1$), we obtain $\vartheta_{ij}^l \approx -1$ and thus the general formula $E_{c_i c_j}^{v_l} \approx -E_{c_i}^{v_l} E_{c_j}^{v_l}$, which is symmetric between substrates and products. For irreversible reactions (with $A_l \rightarrow \infty$ and $\zeta_l \rightarrow \infty$), in contrast, we obtain $E_{c_i c_j}^{v_l} \approx 0$ because the factor $\zeta_l/(\zeta_l - 1)^2$ is close to 0. Can this relationship be expected for other rate laws as well? For general saturable rate laws, a splitting as in Eq. (28) will remain possible formally, but there is no simple formula for ϑ_{ij}^l . Accordingly, the negative correlation between $E_{c_i c_j}^{v_l}$ and $E_{c_i}^{v_l} E_{c_j}^{v_l}$ will become weaker, but a tendency for negative correlations may remain.

D Model construction based on elasticity sampling

Constraints for variables in kinetic steady-state models A kinetic steady-state model, with all elasticities and kinetic constants, is specified by model structure, rate laws, state variables, and saturation values. For a consistent model, these variables have to satisfy a number of constraints:

- *Wegscheider conditions (C1)*. Some biochemical quantities, for instance reaction Gibbs free energies, can be written as differences Δx_l along biochemical reactions. In vector form, they can be written as $\Delta \mathbf{x} = \mathbf{N}^\top \mathbf{x}$, where \mathbf{N} is the stoichiometric matrix including all (internal and external) metabolites, so with a null-space matrix \mathbf{K} satisfying $\mathbf{N} \mathbf{K} = 0$, they must obey the Wegscheider condition $\mathbf{K}^\top \Delta \mathbf{x} = 0$. Wegscheider conditions hold for equilibrium constants ($\ln \mathbf{k}^{\text{eq}} = \mathbf{N}^\top \ln \mathbf{c}^{\text{eq}}$), mass-action ratios ($\ln \mathbf{q}^{\text{ma}} = \mathbf{N}^\top \ln \mathbf{c}$), and driving forces ($\mathbf{A} = -\Delta \boldsymbol{\mu} = -\mathbf{N}^\top \boldsymbol{\mu}$).
- *Haldane relations (C2)*. In chemical equilibrium, all metabolic fluxes v_l vanish. By considering a reaction in equilibrium, setting its rate to zero ($r_l(\mathbf{c}^{\text{eq}}, \dots) = 0$), and solving for the equilibrium constant, we can obtain an equation between equilibrium constant and kinetic constants, the so-called Haldane relation [59]. For a reversible mass-action law $v_l = k_l^+ a - k_l^- b$, the Haldane relation reads $k_l^{\text{eq}} = k_l^+ / k_l^-$. For the modular rate laws, it is given by $k_l^{\text{eq}} = \frac{k_l^+}{k_l^-} \prod_i (k_{li}^{\text{M}})^{h_l n_{il}}$ (see [19]).
- *Equilibrium constant and chemical standard potentials (C3)*. In chemical equilibrium, all chemical potential differences $\Delta \mu_l$ must vanish. With $\mu_i = \mu_i^{(0)} + RT \ln c_i$ (i.e. assuming an activity coefficient equal to 1), this leads to the equalities $\ln k_l^{\text{eq}} = -\frac{1}{RT} \sum_i \mu_i^{(0)} n_{il}$ and $A_l = -\Delta \mu_l = RT \ln \frac{k_l^{\text{eq}}}{q_l^{\text{ma}}}$.
- *Signs of fluxes and driving forces (C4)*. According to the second law of thermodynamics, all chemical reactions must dissipate Gibbs free energy. This implies that rates and driving forces have the same signs ($v > 0 \Rightarrow A > 0$ and $v < 0 \Rightarrow A < 0$), in agreement with the relationship $\ln A/RT = \frac{v^+}{v^-}$. A stricter version of this constraint, excluding equilibrium reactions, is given below.
- *Steady-state fluxes (C5)*. The fluxes in steady state must satisfy the stationarity condition $\mathbf{N}^{\text{int}} \mathbf{v} = 0$. In addition, we may impose bounds $\mathbf{v}^{\text{min}} \leq \mathbf{v} \leq \mathbf{v}^{\text{max}}$ on the reaction rates and bounds $\mathbf{v}_{\text{ext}}^{\text{min}} \leq \mathbf{N}^{\text{ext}} \mathbf{v} \leq \mathbf{v}_{\text{ext}}^{\text{max}}$ on the production or consumption of external metabolites. Such bounds can be used to predefine reaction directions or to keep fluxes close to the experimental values.
- *Amounts and concentrations*. In compartment models, substance balances refer to amounts whereas rate laws depend on concentrations. Although amounts and concentrations are related by (possibly variable) compartment sizes, they can be treated, for the purpose of our model construction, as completely separate quantities. While concentrations appear as model variables, amounts are disregarded except for the fact that they may not change (as required in the stationarity condition for fluxes).

An algorithm for kinetic steady-state modelling must respect these constraints; otherwise it would lead to inconsistent models or states.

Model construction algorithm Given a model and external metabolite concentrations, one could determine a steady state numerically (Figure 9 (a)). However, to guarantee a biochemically plausible state,

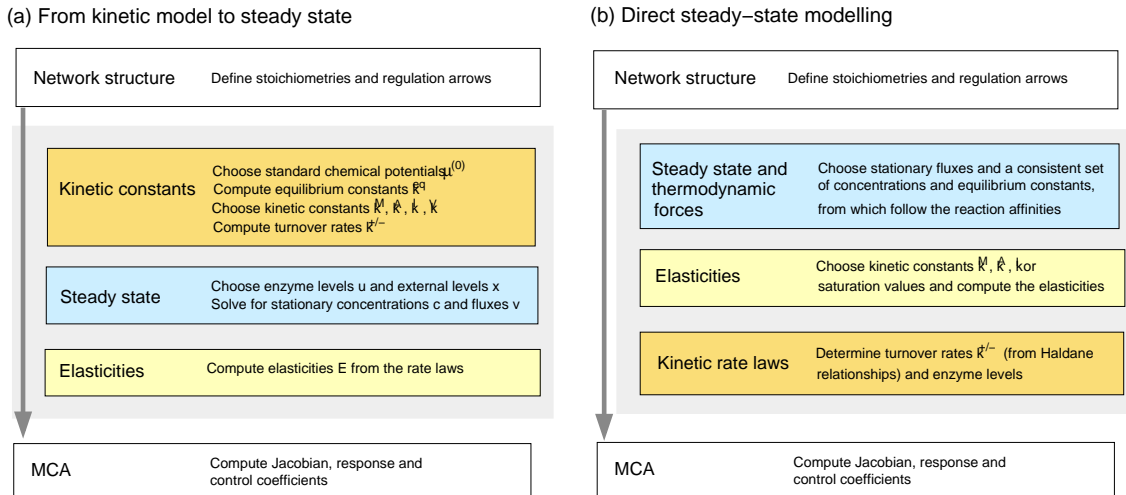


Figure 9: **From metabolic networks to metabolic control analysis.** (a) Forward modelling proceeds from kinetic model to steady state. A kinetic model is defined by network structure and rate laws. Given the rate constants, we can determine a steady state and compute its elasticities by taking the derivatives of the rate laws. The elasticities determine the dynamics close to the steady state and are the basis of Metabolic Control Analysis. (b) Direct steady-state modelling. Steady-state variables (metabolite levels, fluxes, and equilibrium constants) are chosen under thermodynamic constraints. Saturation values or dissociation constants are chosen and the elasticities are computed from them. The free model variables (state variables and saturation values or dissociation constants) can be independently chosen, sampled, or optimised based on predefined values, bounds, or probability distributions.

it is easier to directly predefine the stationary fluxes and to choose kinetic rate laws and metabolite levels that match them by construction (Figure 9 (b)). Model construction based on elasticity sampling combines ideas from thermodynamic flux analysis [60, 7, 9] (steady-state phase) as well as SKM [30] and thermodynamically feasible model parametrisation [18, 55] (elasticity phase). Like in SKM, steady-state concentrations and fluxes can be predefined. To satisfy Wegscheider conditions, Haldane relations, and the sign constraints between reaction rates and driving forces, steady-state quantities and kinetic constants are chosen sequentially. The network structure, our starting point, is defined by a stoichiometric matrix, an allosteric regulation matrix, and a list of external metabolites. Then, free variables (steady-state variables and saturation values) are determined step by step and based on known values, constraints, or probability distributions. In practice, free values can be chosen manually, by optimisation, by fitting them to data, or by random sampling. The dependent variables (e.g. rate constants) are computed from previously chosen variables according to the dependence scheme shown in Figure 2. Details about specific models and their construction are given in section G. All models in the article were checked for stability of the reference state.

A common procedure in the steady state phase is to choose a flux distribution by flux minimisation and to determine metabolite concentrations, Gibbs free energies of formation, and driving forces using parameter balancing [54], using upper and lower bounds for concentrations and driving forces, known values (for concentrations) and predicted values (for Gibbs free energies of formation) as data, and flux directions as inequality constraints. The upper and lower bounds, signs, inserted values, and distributions used in

sampling reflect model assumptions and available data; in choosing them, we can adjust the model to specific metabolic states and to kinetic or metabolic data. Fluxes and driving forces may be sampled uniformly with linear constraints and with predefined sign patterns; metabolite levels, enzyme levels, and dissociation constants may be sampled from log-normal distributions, and saturation values may be sampled from uniform or beta distributions. Free matlab code, using the sparse tensor toolbox [61, 62] is available at https://github.com/wolframliiebermeister/elasticity_sampling.

Reconstruction of kinetic rate laws from state variables and elasticities The scaled elasticities in elasticity sampling are not directly given by saturation values as in SKM, but are computed from them and from the known driving forces. Each sampled set of elasticities corresponds to a specific kinetic model with consistent rate constants. In a variant of the algorithm, we do not sample the saturation values (β_{li}^M , β_{li}^A , β_{li}^I), but the dissociation constants (k_{li}^M , k_{li}^A , and k_{li}^I). In both cases, the catalytic constants k^\pm are computed from two constraints: the Haldane relations determine the ratio k_i^+/k_i^- , so both could still be proportionally scaled. For choosing the scaling, we either predefine the enzyme levels u_l and scale the catalytic constants k^\pm such that the reaction rate matches the predefined flux; or we predefine the k^\pm values and solve for the enzyme levels.

Finally, the rate laws of some reactions may be replaced by laws obtained from enzyme assays to make the model more accurate [63]. For a consistent model, fluxes, concentrations, and equilibrium constants must match between these rate laws and the larger model. Therefore, either the numbers from the rate law must be used as constraints during elasticity sampling, or the rate constants and enzyme level in the rate law must be adjusted to match the numbers from the network model².

Our models represent samples from an ideal, infinitely large model ensemble defined by three aspects: (i) restrictions on model structure and steady state, set by the modeller (e.g., the choice of a fixed flux distribution); (ii) the independence between the free variables and the way in which other variables depend on them as encoded in the dependence scheme (Figure 2); (iii) the random distributions from which the free variables are sampled. These choices define the distributions and statistical dependencies of all model variables, and any kinetic model satisfying the constraints can be obtained by the algorithm.

Extensions of the algorithm The algorithm for model construction can be extended in various ways:

- *Compartments.* In kinetic models with compartments, compartment sizes appear in the balance equations and may, themselves, follow differential equations. In our model construction, compartments are not explicitly modelled, but a compartment structure can be added to the reconstructed kinetic model. This, however, will change the control properties such as Jacobian, response, and control matrices.
- *Dilution by cell growth.* In models with dilution (by growth rate κ), each intracellular metabolite will be effectively degraded with a dilution flux κc_i . This changes the conditions for stationary fluxes and directly couples them to the metabolite levels. Given the steady state, the elasticities can be computed as normally, but the Jacobian, response, and control coefficients will be affected. The

²With irreversible rate laws, the equilibrium constant can obviously disregarded

elasticities for the dilution reactions themselves are directly given by dilution rate and metabolite levels.

- *Thermodynamically inconsistent fluxes.* Eq. (1), the central formula in elasticity sampling, requires that all fluxes lead from higher to lower chemical potentials. In practice, a given flux distribution may violate this assumption, for instance, if cofactors or protons are omitted in the reaction formulae or if cell compartments are disregarded. To apply elasticity sampling in such cases, we need to adjust the driving forces: whenever a flux sign differs from $\text{sign}(-\Delta\mu_l)$, we assume a virtual external substrate whose chemical potential μ_x leads to a driving force $-\Delta\mu^* = -(\Delta\mu_l + \mu_x)$ with the right sign. The virtual substrate changes the equilibrium constants and driving forces, but can be ignored in the kinetic rate law.
- *Avoiding divergencies close to chemical equilibrium.* In reactions with small driving forces A_l , microscopic rates v_l^\pm and scaled elasticities can become extremely large. This is not only problematic numerically, but also implausible because reactions with a finite flux, but close to chemical equilibrium would require very fast or abundant enzymes. To avoid this in our models, we set a constraint $v_l^\pm < \rho |v_l|$ on the forward and reverse rates in each reaction. With a threshold $\rho = 100$, for instance, forward fluxes could be at most 100 times as large as the net flux. This can be turned into a constraint for driving forces in the steady-state phase: the flux sign constraint $C4 (v_l \neq 0 \Rightarrow \text{sign}(v_l) A_l \geq 0)$ is replaced by the tighter constraint³ $v_l \neq 0 \Rightarrow \text{sign}(v_l) A_l \geq RT/\rho$. It will prevent extreme values in the thermodynamic elasticity term E_{li}^{rev} . The unscaled elasticities, in contrast, do not diverge in chemical equilibrium and can be directly computed from non-divergent formulae [19].
- *Enzyme reactions composed of elementary steps.* Enzymatic mechanisms can be split into elementary steps with mass-action kinetics. If a model has this form, all rate laws are mass-action kinetics, the elasticities are directly given by the reversibility terms and are thus fully determined by the driving forces from the steady-state phase. In this case, a choice of fluxes and driving forces will completely determine the enzyme kinetics; this may be surprising, but one need not forget that the driving forces describe *elementary steps*, whose equilibrium constants correspond to the k^M values of the saturable modular rate laws, and that each flux through such an elementary steps defines one of the maximal velocities.
- *Prior distributions for saturation values.* Saturation values $\beta = k/(k+x)$ can be given fixed values (e.g., $\beta = 0$ for enzymes in the linear range, $\beta = 1/2$ in half-saturation, or $\beta = 1$ in full saturation) or be sampled independently from the range $]0, 1[$. If β is drawn from a uniform distribution (as suggested by the principle of minimal information [64]) and the metabolite levels are fixed, the dissociation constant k will be randomly distributed with probability density $p(k) = \frac{k}{(c+k)^2}$ (see SI I.1). If a saturation value is approximately known, we can also use a beta distribution with density $p(\beta) \sim \beta^{a-1}(1-\beta)^{b-1}$, with mean $a/(a+b)$ given by the known value. This yields a distribution $p(k) = \frac{k}{(c+k)^2} \left(\frac{c}{k+c}\right)^{a-1} \left(\frac{k}{k+c}\right)^{b-1} = \frac{k^{b-1} c^{a-1}}{(k+c)^{a+b}}$ for the dissociation constant. Saturation values could also be sampled from dependent distributions: this may be necessary if enzymes bind to different

³The constraint can be derived as follows (assuming $v_l > 0$ without loss of generality): the ratio between forward and net reaction rate reads $v_l^+/v_l = \zeta_l/(\zeta_l - 1)$. Close to equilibrium, we can approximate $1/\zeta_l \approx 1 - A_l/RT$ and obtain $\rho \geq \frac{v_l^+}{v_l} = \frac{1}{1-1/\zeta_l} \approx RT/A_l$.

reactants, for instance NAD^+ und NADH , with unknown but similar binding affinities, leading to correlations between their saturation values in physiological states.

- *Analysis of sampled output variables.* Mathematically, a model ensemble can be seen as a statistical model with independent (“free”) and dependent (“determined”) variables and with dependencies as in Figure 2. Each qualitative property (e.g., the sign of a control coefficient) has a certain probability in the ensemble. In practice, we need to estimate this probability from a limited number of model instances sampled. If n out of N sampled models show some property P , the true probability of P , called q , can be estimated as follows: assuming that q has a uniform prior, its posterior mean and variance read $\mu_q = \frac{n+1}{N+2}$ and $\sigma_q^2 = \frac{(n+1)(N-n+1)}{(N+2)^2(N+3)}$. For each quantitative output variable (e.g., a control coefficient), we obtain a number of sampled values. Their distribution can be statistically analysed in terms of mean, variation, probabilities of signs, and correlations with other model variables.
- *Significant differences between model variants.* By subsequent, nested choices of network structure, fluxes, driving forces, and enzyme saturation, we can create a hierarchy of model variants. Each model variant is represented by a model ensemble with a specific distribution of output variables. To allow for comparisons, model variants should have the same metabolite and reaction lists, but they can differ in their network structures and in the values of any free variables (for details, see SI H.2). Significant differences between the distributions of model outputs can be found by statistical tests, if necessary with corrections for multiple testing (see SI H.2). By comparing the distribution of model variables between subensembles, we can check how output variables are affected by structural model features: for instance, whether the stability of steady states can be enhanced by certain allosteric regulation arrows. More generally, we can systematically dissect the effects of network structure, allosteric regulation, thermodynamic forces, enzyme saturation, and different rate laws on our model outputs.
- *Controlling the output variables during model building.* To enforce certain values or distributions of output variables, we can filter the model ensemble for appropriate models and obtain a subensemble with different distributions and correlations of the model variables. Even free variables, which were chosen independently, can become dependent by the subselection. Alternatively, we can control the distribution our output variables during model construction by Bayesian posterior sampling: the free variables are not sampled freely, but according to a Metropolis Monte Carlo procedure: as priors, we can choose the usual probability distributions; for the likelihood function, we compare the resulting output variables to the prescribed distribution, for instance, a distribution defined by experimental data.
- *Multiple steady states.* Depending on the external metabolite levels and enzyme levels, a kinetic model can show steady states with different metabolite levels, fluxes, saturation values, and elasticities. For constructing a model with several steady states, the algorithm needs to be modified in order to ensure that all saturation values and elasticities correspond to the same set of rate constants. In the steady-state phase, we sample a set of equilibrium constants and multiple steady states; in the elasticity phase, we sample a single set of rate constants, which then determine the saturation values, elasticities, and enzyme levels for each of the steady states. The enzyme levels are fully determined

by the other variables; the only way to control them – e.g. for adjusting them to proteome data – would be to run the entire algorithm as a parameter fitting or posterior sampling.

- *Adaption of enzyme levels.* Enzyme levels, which appear as parameters in our models, are in reality controlled by transcriptional regulation, and adaption of enzyme levels is an important factor shaping metabolic long-term responses. Since transcriptional enzyme regulation is not part of our metabolic models, these effects cannot be handled directly unless gene expression is explicitly incorporated into the metabolic model. However, plausible enzyme adaption profiles may be derived from optimality considerations [37]. To allow metabolism to run efficiently, enzymes should be expressed in the right proportions and according to the current metabolic task. For instance enzymes in the synthesis pathway may be induced simultaneously as the demand for the pathway product rises. Likewise, changes in an enzyme level – for whatever reason – will affect the metabolic state and may induce secondary adaptations of other enzyme levels, and so on. When predicting the effects of, e.g., single-gene knock-downs, it can be important to consider the global interplay of such adaptations. Given a kinetic model, a metabolic target, and an enzyme cost function, optimal enzyme adaptations to external changes or to single-enzyme knock-downs can be computed from the second-order response coefficients. The predicted enzyme adaptations will reflect both network structure and elasticities.

E Synergies between enzyme perturbations

Synergies are of medical importance, to anticipate drug interactions and patient-specific side effects, to develop efficient combination therapies, and to fight the emergence of bacterial resistance [65]. A well-studied example of synergies is epistasis, the synergistic effects of gene knockouts on the viability of cells. Epistasis is an important factor shaping genetic variability in populations and genetic changes in evolution. As shown by experiments and FBA simulations, it can indicate functional associations between proteins and in particular the involvement of enzymes in metabolic pathways [44].

Epistasis Epistasis describes the synergy effects of gene deletions on the Darwinian fitness. Such synergisms play an important role in population genetics because they can influence the evolution of genomes: in buffering epistasis between two genes (double-deletion phenotype is less severe than expected), the loss of one gene will lower the selection pressure on the other, so the genes will tend to be either both present or both absent in genomes, leading to phylogenetic correlation [66]. In aggravating epistatic synergies (double-deletion phenotype is more severe than expected), the loss of one gene will increase the selection pressure on the other, leading to phylogenetic anti-correlation. In [44], epistatic synergies in the yeast *S. cerevisiae* were computed by FBA. The maximal possible biomass production rate was used as a quantitative output function and enzyme deletions were simulated by setting the corresponding reaction rates to zero. The epistasis pattern turned out to be modular, corresponding to a functional classification of genes into metabolic pathways: the epistatic synergies across such enzyme groups showed consistent signs and were therefore called “monochromatic” [44].

Epistasis measure by Segré et al. Segré *et al.* introduced a special synergy score to quantify the epistatic effects between double enzyme deletions [44]. This measure reweights buffering synergies to

make them clearly detectable. Let v_{wt} denote the output variable (e.g. maximal biomass production rate in FBA) for the wildtype network and v^a , v^b , and v^{ab} the values for networks in which enzyme a, enzyme b, or both are deleted. Scaled by the wildtype value, the output values read $w_{\text{wt}} = 1$, $w_a = v^a/v_{\text{wt}}$, $w_b = v^b/v_{\text{wt}}$ and $w_{ab} = v^{ab}/v_{\text{wt}}$. Since deletions can decrease but not increase the output in FBA, the values satisfy $w_a \leq 1$, $w_b \leq 1$, and $w_{ab} \leq \min(w_a, w_b)$. An epistasis score compares the effect w_{ab} of a double deletion to the effects w_a and w_b of single deletions. To be able to clearly distinguish between neutral ($w_{ab} = w_a w_b$), aggravating ($w_{ab} < w_a w_b$), and buffering ($w_{ab} > w_a w_b$), gene pairs, Segré *et al* introduced a heuristic epistasis measure with the following definition:

$$\bar{\varepsilon}^{ab} = \begin{cases} \text{neutral} & : 0 \\ \text{aggravating} & : \frac{w_{ab}}{w_a w_b} - 1 \\ \text{buffering} & : \frac{w_a w_b - 1}{\frac{1}{w_b} - 1} \end{cases} \quad (30)$$

In the third formula, we assume $w_a \leq w_b$ without loss of generality. In summary, neutral and aggravating synergies are counted “normally”, but buffering synergies are weighted: if one of the single-deletion effects is mild, then w_b is close to 1 and the buffering synergy is increased by this definition. If both single deletions are already severe, then the buffering synergy is downweighted.

Synergies predicted by FBA and MCA FBA, MoMA, and MCA predict enzyme synergies based on different types of assumptions and input data. Both methods confirm the general sense that, in the case of double inhibition, cooperating enzymes (i.e. enzymes within a linear pathway) tend to show buffering synergies and enzymes engaged in alternative pathways show aggravating synergies. However, the reasons for these predictions, their details, and other predictions differ. Example predictions for a simple pathway are shown in Figure 5. As expected, inhibiting both routes simultaneously has an aggravating effect. In MCA, the reason is that inhibition of one branch will increase the flux control of the other branch. In contrast, different enzymes along a chains show buffering synergies. In this case, a first inhibition takes away flux control from the other enzymes. In the graphics, significance values were thresholded (values below one percent of the maximal synergy value are not shown).

F Metabolic fluctuations

Computing the fluctuations caused by chemical noise The external perturbations affecting a pathway can be dynamic; if they are modelled as random processes, the perturbations and the resulting metabolite fluctuations can be described by spectral power density matrices, which resemble the static covariance matrices, but are frequency-dependent. If the noise amplitudes are small, we can use a linearised model and compute the spectral densities of fluctuating metabolite levels from the spectral response coefficients [39]

$$\mathcal{S}_c(\omega) = \mathbf{R}^s(\omega) \mathcal{S}_p(\omega) \mathbf{R}^{s\dagger}(\omega). \quad (31)$$

$S_c(\omega)$ and $S_p(\omega)$ denote the spectral power densities of metabolites and perturbation parameters at circular frequency ω , the symbol \dagger indicates the adjoint matrix, and the unscaled first-order spectral response matrices $\mathbf{R}^s(\omega)$ and $\mathbf{R}^j(\omega)$ follow from the elasticities [38, 39]. Fluctuations of reaction rates can be treated with an analogous formula.

Chemical noise is a good example: microscopically, chemical reactions are not continuous processes, as assumed in kinetic models, but discrete random events. Under simplifying assumptions, this random dynamics can be described by a Langevin equation, i.e., a kinetic model with additive white noise in the forward and reverse reaction rates [46]. The rate fluctuations spread in the network according to the model dynamics, leading to permanent fluctuations of molecule numbers in the macroscopic steady state. The prefactor in the noise term scales with the square root of the mean reaction rate (in units of reaction events per second). Therefore, noise will play a bigger role for smaller particle numbers, and if the mean rates become too small, the approximation breaks down. The fluctuations can be described by Eq. (31), setting $E_{p_{l^*}} = \sqrt{\frac{v_{l^*}}{N_A \Omega}}$ (where $*$ marks microscopic fluxes) and $S_p(\omega) = \mathbf{I}$, because they originate from white noise (see [39]). In practice, the spectral power density of the original noise in reaction l is given by

$$S_p(\omega) = \frac{v_l^+ + v_l^-}{N_A \Omega} = \frac{\coth(h_l A_l / RT) v_l}{N_A \Omega} \approx \frac{RT}{N_A \Omega} \frac{v_l}{h_l A_l} \quad (32)$$

where the approximation holds close to equilibrium (small A_l). The dynamic system translates these “input” fluctuations into “output” fluctuations of metabolite levels and fluxes (for an example, see Fig 11). Fast fluctuations will be strongly damped, so the noise spectrum of the metabolite levels decreases at high frequencies and the system acts as a low-pass filter. Since reaction fluxes are directly affected by their own noise, they also fluctuate at high frequencies. If a system tends to oscillate, noise may become amplified around certain resonance frequencies; all this can directly be seen from the eigenvalue spectrum of the Jacobian matrix [39].

Limiting behaviour of spectral power densities at high or low frequencies For very high or low frequencies, the spectral power densities show a simple limiting behaviour. The spectral power density for metabolite fluctuations has the form $\mathbf{R}^s(\omega) \mathbf{M} \mathbf{R}^{s\dagger}(\omega)$ with some diagonal matrix \mathbf{M} . The spectral power densities are given by diagonal values

$$\sum_p \|R_p^c(\omega)\|^2 m_p. \quad (33)$$

The spectral response matrix has the form $\mathbf{R}_p^c(\omega) = \mathbf{A} (\mathbf{J} - i\omega \mathbf{I})^{-1} \mathbf{B}$. For large frequencies (ω much larger than any eigenvalues of the Jacobian \mathbf{J}), the term $i\omega \mathbf{I}$ dominates and the entire expression (33) becomes proportional to $\frac{1}{\omega^2}$. The high-frequency noise is dominated by the direct effects of rate fluctuations on the adjacent reactant levels, i.e., non-stationary deviations from the stationary fluxes. On the contrary, for low frequencies, the spectral power density approaches the variability expected for static variability, and the correlations correspond to variations of the stationary fluxes.

Fluctuations on different timescales The spectral power densities describe noise components at specific frequencies. For a more intuitive measure of slow or fast noise, we can consider the noisy curve, compute

a sliding average with a certain time window (e.g. one second), and see how much this average varies over time. From the spectral power densities, the variation of concentrations, observed on different time scales, can be computed with the help of Fourier transformations: we consider a sliding average with a Gaussian kernel (of width τ) and compute the variance as described in section I.3.

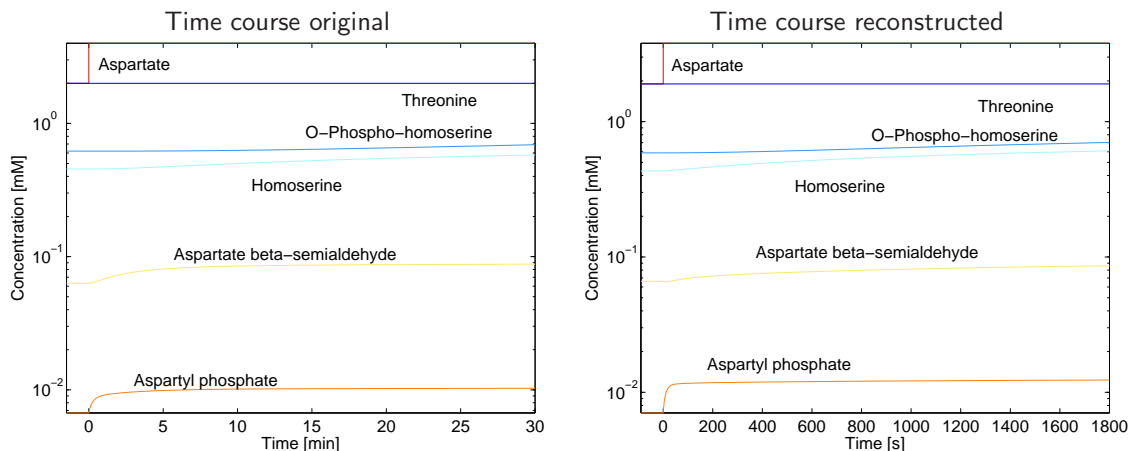
G Example models

(1) Glycolysis in human hepatocytes Control analysis of ATP rephosphorylation flux Thermodynamically feasible fluxes had been determined in [40] by flux minimisation with a single flux objective, in the case shown the rephosphorylation of ATP under glucose and oxygen consumption. Within the large original network, the reduction to this task leads to a sparse flux distribution covering only a small part of the network in particular glycolysis and the TCA cycle. For simplicity, the saturation values were not sampled, but set to values of 1/2, assuming that all enzymes are half-saturated. In the example, the ATP stationary ATP level is strongly controlled by glucose import; all control coefficients are positive, i.e., small increases of any enzyme would increase the metabolic output (ATP level). Although the flux distribution with initially chosen to support ATP rephosphorylation, this is not trivial for two reasons: first of all, flux analysis can capture the ATP rephosphorylation rate, but not the ATP level as a target function; second, it describes which fluxes – and in which proportions – are optimal to realise a certain metabolic objective, but not the marginal effects of enzyme levels, i.e., how the objective would change upon small enzyme changes. By sampling the saturation values, a model ensemble could be obtained and the statistical distribution and correlations of these control coefficients could be studied.

(2) Dynamic responses – comparison to original kinetic models To test whether elasticity sampling leads to realistic models, the two models were downloaded from Biomodels Database. Using the network given topologies, new kinetic models were reconstructed by parameter sampling, based on steady-state fluxes and concentrations of the original models. As a perturbation, models were considered in an initial steady state, then the external substrate level (aspartate for the threonine pathway, glucose for glycolysis) was increased and then kept constant.

(3) Effect of driving force and saturation on control and fluctuations The effect of driving force and saturation on control and fluctuations, for a simple pathway model are shown in Figure 11. The pathway is a chain of five uni-uni reactions without allosteric regulation. In a standard version of the model, all driving forces were set to RT and all saturation values to 1/2. Then, the values for the third reaction were systematically varied, setting the force to values of 0.1 RT, RT, and 10 RT, and the saturation values to 0.1, 0.5, and 0.9. The figure shows, both for metabolite levels and fluxes, the static control coefficients and the spectral power densities of chemical noise. Some clear patterns are visible: If the reaction is close to equilibrium (0.1 RT), it exerts little concentration and flux control and does not strongly affect the control exerted by other reactions. On the contrary, if the reaction becomes more, it exerts a larger control. At the same time, the control exerted by downstream enzymes, and all control on downstream metabolites decreases. For the reaction close to equilibrium, the substrate saturation does not play a role; as the reaction becomes more irreversible, the substrate saturation additionally increases the control exerted

(a) *E. coli* threonine pathway (perturbation: increase of aspartate level)



(b) Hepatocyte glycolysis (perturbation: increase of external glucose level)

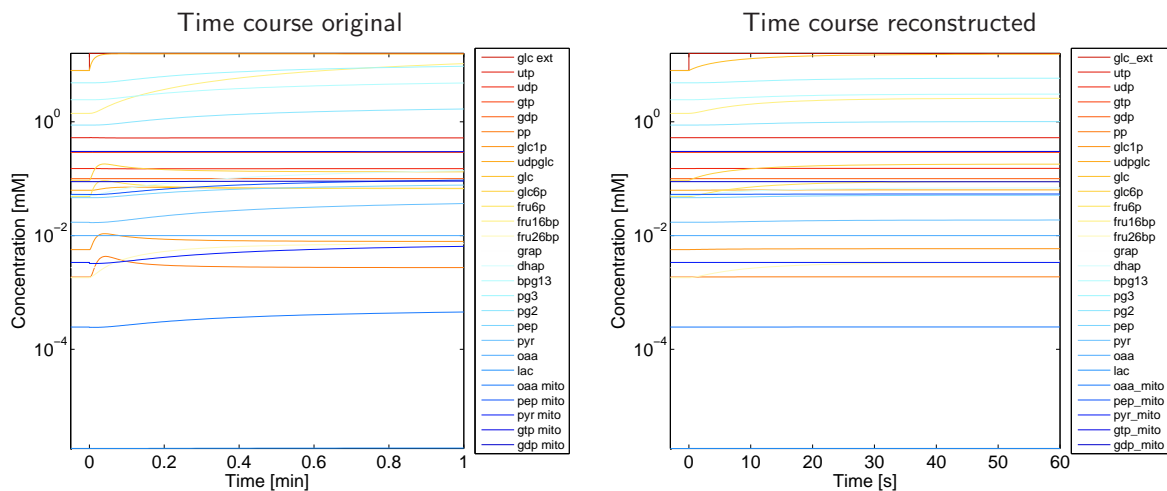
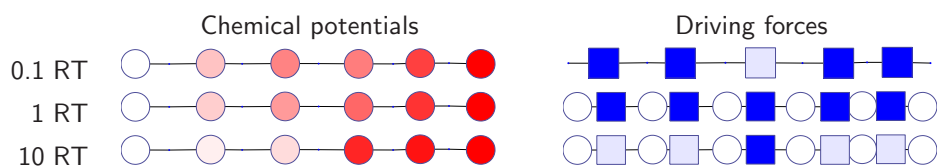


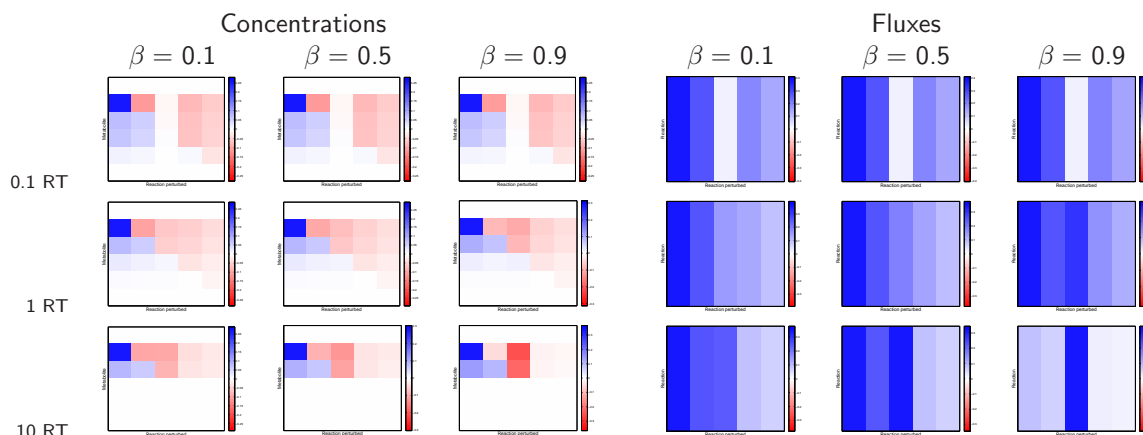
Figure 10: **Dynamic simulations of kinetic models obtained by elasticity sampling.** (a) Model of the threonine synthesis pathway in *E. coli* [41]. The pathway converts aspartate to threonine; a sudden increase in the the external aspartate level, the intermediate levels increase subsequently. Left: Simulation of the original model from [41]. Right: Simulation of the reconstructed model, constructed by elasticity sampling based on a steady-state of the original model. (b) Kinetic model of glycolysis in human hepatocytes [42], simulations for an increase of the external glucose level. While the dynamic of the threonine pathway is well approximated, the overshoot in the hepatocyte glycolysis was not recovered by the reconstructed model. Nevertheless, the time scale of changes is on the right order of magnitude.

by the reaction. Thus, the highest control is exerted by if the reaction is irreversible and the enzyme is saturated with substrate.

(a) Variation of driving forces



(b) Control coefficients



(c) Spectral power densities

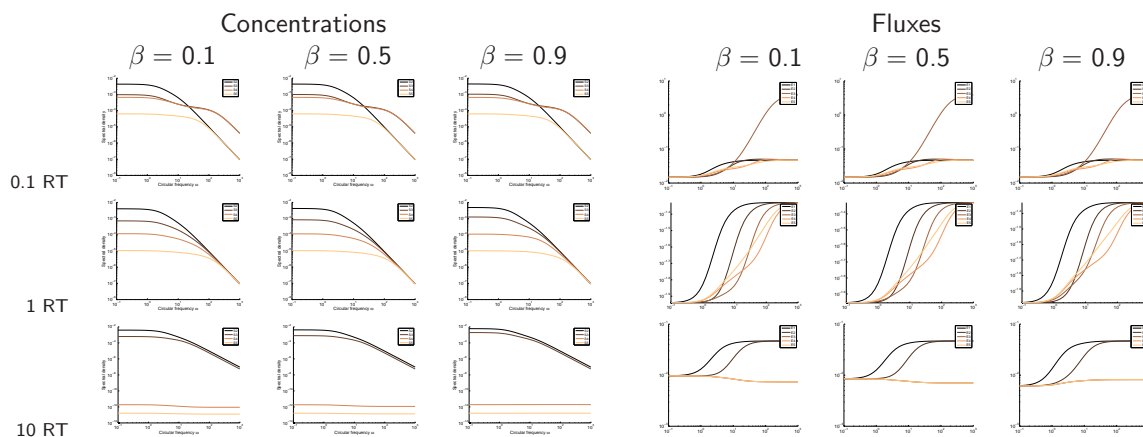


Figure 11: **Thermodynamic force, control, and noise in a linear chain.** Model versions with different driving forces (0.1 RT, RT, 10 RT) and saturation values (0.1, 0.5, 0.9) in the central reaction were constructed. (a) By varying the chemical potentials (left; white: high; red: low), the thermodynamic driving force of the central reaction was made weaker, equal or stronger than in the other reactions. (b) Static concentration and flux control coefficients for the different model variants. (c) Concentration and flux spectral power densities (fluctuations caused by chemical noise) for the different model variants.

H Calculation methods

H.1 Varying the driving forces for a given flux distribution

To assess the specific influence of the thermodynamic forces on model behaviour, we may need to vary all thermodynamic forces, while keeping a fixed flux distribution. A variation of thermodynamic forces (e.g., making all forces twice as large) will entail a variation of metabolite levels. However, the choice of metabolite concentrations is not unique. As a pragmatic procedure, we suggest the following: we start from an initial metabolic state with concentration vector \mathbf{c}^{orig} and force vector \mathbf{A}^{orig} (which needs to agree with the flux directions). A varied force vector \mathbf{A} (which has to show the same signs as \mathbf{A}^{orig}) is realised by a new concentration vector \mathbf{c} chosen as follows:

$$\begin{aligned} \mathbf{c} &= \operatorname{argmin}_{\mathbf{c}} \|\ln \mathbf{c} - \ln \mathbf{c}^{\text{orig}}\|^2 \\ \text{s.t. } \mathbf{A} - \mathbf{A}^{\text{orig}} &= -RT \mathbf{N}^{\text{int}\top} [\ln \mathbf{c} - \ln \mathbf{c}^{\text{orig}}] \end{aligned} \quad (34)$$

That is, the new pattern of driving forces is to be accomplished at a minimal change of the metabolite concentrations (in the Euclidan sense). Additional upper and lower limits for \mathbf{c} may be imposed, but these may render the problem unsolvable.

H.2 Significant differences between model ensembles

A recurrent question in systems biology is whether dynamic features of a model can be attributed to the network structure, or whether they mostly depend on quantitative factors like the rate constants. More generally, we may consider two model variants that differ in some aspect (e.g., network structure or flux distribution), while other aspects (e.g., rate constants) can still be varied for each of the variants, and ask whether some model output differs significantly between the variants. To prove or disprove such a hypothesis, we can describe both model variants by model ensembles, sample instances of them, compute their output variables, and compare them by significance tests. This, for instance, allows us to compare two variants of a kinetic model (with different network structures, allosteric synergies, steady-state fluxes, or expression patterns) and to check whether these differences lead to typical differences in their synergy patterns, irrespective of a variation of kinetic parameters.

Binary output variables If we are interested in a qualitative model property (e.g., is the steady state stable or unstable?), a model ensemble can be characterised by the fraction p of “positive” model instances. Given a number of sampled model instances (with count numbers n_+ and n_- for “positive” and “negative” model instances), the true fraction p can be estimated by Bayesian estimation. If p were the true fraction, the number n_+ of positive model instances (out of $N = n_+ + n_-$ model instances sampled) would be binomially distributed with mean pN and maximal value N . On the contrary, the value of p can be estimated from the given number n_+ using Bayesian estimation. Assuming a flat prior, the posterior of p is a beta distribution $\operatorname{Prob}(p) \sim p^{\alpha-1}(1-p)^{\beta-1}$ where $\alpha = n_+ + 1$ and $\beta = N - n_+ + 1$. The mean value of this distribution, $\langle p \rangle = \alpha/(\alpha + \beta) = (n_+ + 1)/(N + 2)$ can be used as an estimator for p . The corresponding variance reads $\sigma_p = \frac{\alpha\beta}{(\alpha+\beta)^2(\alpha+\beta+1)} = \frac{(n_++1)(N-n_++1)}{(n_{\text{perm}}+2)^2(N+3)}$.

A statistical score for the bias of synergy signs. Given a matrix of enzyme synergies, and after removing small-magnitude values by thresholding, we count the positive and negative synergies (numbers n_+ and n_-) between two enzyme groups, e.g., between enzymes involved in two metabolic pathways. As a null hypothesis, we assume that each synergy can be positive or negative, with equal probabilities. Under the null hypothesis, and assuming that there are only very few synergies after thresholding, n_+ and n_- would be independently binomially distributed with the same unknown mean value n . Given n , the difference $n_+ - n_-$ would have mean 0 and standard deviation $\sqrt{2n}$. Thus, ratio between an observed difference and this standard deviation can be used as a score for sign bias. Since the value of n is unknown, we approximate it by $\frac{n_+ + n_-}{2}$ and obtain the empirical sign bias score $z_{\text{sign}} = \frac{n_+ - n_-}{\sqrt{n_+ + n_-}}$.

Quantitative output variables Now, we turn towards quantitative output variables and differences between different model variants, represented by model ensembles. As an example, we consider computed enzyme synergies. The general logic is as follows. To see whether a synergy value differs between two model variants, we compute the synergies for many model instances and consider the mean values for both model variants: we compare these two values and use a p-value (obtained from a permutation test) as a criterion for them being different. Since we run such tests for many enzyme pairs in parallel, we can expect a potentially large number of false positives. To account for this typical multiple testing issue, we select “significant” enzyme pairs based on their p-values and on a predefined false discovery rate [67]. This is how the procedure works in detail:

1. **Sample synergy values** For each of the two model variants, we sample n_{model} model instances. For each model instance, we compute the synergies for all enzyme pairs. Thus, we obtain a large collection of synergy values η_{ijk} , indexed by $i \in 1, \dots, n_{\text{pairs}}$ for enzyme pairs, $j \in \{1, 2\}$ for model variants, and $k \in 1, \dots, n_{\text{inst}}$ for sampled model instances of each variant. If the network contains n_r enzymes, there are $n_{\text{pairs}} = n_r(n_r - 1)/2$ enzyme pairs, i.e., possible synergies to be considered. These data will now be tested for significant differences.
2. **Quantify large (positive or negative) synergies by p-values** First, we can test, for each enzyme pair i , if it shows a large synergy values caused by the model structure. If this is the case, the synergy value stand out from the general distribution of synergy values even if we average over many random choices of the kinetic parameters. We apply the following statistical test: For each enzyme pair a , we test if the mean value $\eta_{i..}$ (from both model variants and all Monte Carlo samples) is significantly larger or smaller than other synergy values. To do so, we use a permutation test: the actual mean value $\eta_{i..}$ for our enzyme pair is compared to mean values obtained from batches of resampled η_{ijk} values. In each permutation run $l \in 1, \dots, N$, we resample $2 \cdot n_{\text{inst}}$ of the η_{ijk} values with replacement and compute their mean value $\bar{\eta}_{il}$. Let n_i denote the number of resampled mean values $\bar{\eta}_{il}$ larger than $\eta_{i..}$. Whether $\eta_{i..}$ is significantly large is indicated by a p-value p_i , which can be estimated by

$$p_i = \frac{n_i + 1}{N + 2} \quad (35)$$

(for a justification, see the above treatment of binary variables). Small values $p_i \approx 0$ indicate that $\eta_{i..}$ is much larger than expected by chance (i.e., significantly large), large values $p_i \approx 1$ indicate that it is much smaller than expected by chance (i.e., significantly small).

3. **Quantify differences in synergies (between model variants) by p-values** Next, we can ask, for each enzyme pair i , if the synergy values differ significantly between the model variants. To test this, we consider the mean values $\eta_{i1.}$ and $\eta_{i2.}$ of both variants, averaged over all kinetic parameter samples, and check whether they are significantly different. Again, we use a permutation test. This time, we compute the mean difference $\Delta\eta_{ij} = \eta_{i1.} - \eta_{i2.}$. In each run d of the the permutation test, we randomly permute the values η_{ijk} for the pair a under study, subdivide them into two batches of size n_{inst} , and compute the mean difference $\Delta\bar{\eta}_{il}$ between the two batches. A p-value, stating whether $\Delta\eta_{ij}$ is large, for is computed as above, by counting how many of the permutation samples lead to larger values.
4. **Select significant synergies or differences based on p-values** Given the p-values computed so far, we determine which mean values $\eta_{.j.}$ and mean differences $\Delta\eta_{.j.}$ are significantly high (or low). Since we test this for each of the n_{pairs} gene pairs, we need to account for multiple testing: to do so, we fix an envisaged false discovery rate of 5% and choose the confidence level $\alpha = 0.05$ for the individual tests. With this choice, $\alpha \cdot n_{\text{pairs}}$ of the apparently significant values (for each of the four tests, high or low mean synergy and difference in synergy) are expected to be false positives.

I Proofs and derivations

I.1 Probability distributions for saturation values and dissociation constants k^X

The binding between an enzyme and a reactant or regulator depends on the compound's concentration c and the dissociation constant k (indices omitted for simplicity). We can characterise it by saturation values $\alpha = \frac{1}{1+c/k} = \frac{k}{k+c}$ or $\beta = \frac{c}{k+c} = 1 - \alpha$. The saturation value, on the one hand, and c and k , on the other, are directly related. If we sample α (or, equivalently, β) uniformly from the interval $]0, 1[$, the corresponding probability densities (assuming that either k or c are kept fixed) read

$$p(c) = \frac{k}{(k+c)^2} \quad \text{for fixed } k \quad (36)$$

$$p(k) = \frac{c}{(k+c)^2} \quad \text{for fixed } c. \quad (37)$$

Proof: The probability density of α is $p(\alpha) = 1$. For fixed k , we obtain $\partial\alpha/\partial c = -k/(c+k)^2$ and obtain

$$p(c) = C p(\alpha) \left| \frac{\partial\alpha}{\partial c} \right| = C \frac{k}{(k+c)^2} \quad (38)$$

with normalisation constant $C = 1$ because

$$1/C = \int_0^\infty \frac{k}{(c+k)^2} dc = \frac{-k}{k+c} \Big|_0^\infty = 1 \quad (39)$$

For fixed c , we compute $\partial\alpha/\partial k = k/(c+k)^2$ and obtain

$$p(k(\alpha)) = C p(\alpha) \left| \frac{\partial\alpha}{\partial k} \right| = C \frac{c}{(k+c)^2}, \quad (40)$$

again with normalisation constant $C = 1$ because

$$1/C = \int_0^\infty \frac{c}{(k+c)^2} dk = \frac{k}{c+k} \Big|_0^\infty = 1. \quad (41)$$

1.2 Metabolic control and response coefficients

First-order metabolic control and response coefficients Control and response coefficients describe the effects of small parameter changes on state variables (metabolite concentrations s_i and reaction rates j_l) in first- or second-order approximations [33, 34]. The unscaled response and control coefficients can be computed from the unscaled elasticities and the stoichiometric matrix [39]: In systems without conservation relations, the first-order unscaled control matrices read

$$\bar{\mathbf{C}}^s = -(\mathbf{N}^{\text{int}} \bar{\mathbf{E}}_c)^{-1} \mathbf{N}^{\text{int}} \quad (42)$$

$$\bar{\mathbf{C}}^j = \mathbf{I} + \bar{\mathbf{E}}_c \bar{\mathbf{C}}^s. \quad (43)$$

In models with linear conservation relations, the Jacobian $\mathbf{N}^{\text{int}} \bar{\mathbf{E}}_c$ will not be invertible. In this case, we compute the control coefficients via a choice of independent internal metabolites [58]. The stoichiometric matrix is split into a matrix product $\mathbf{N}^{\text{int}} = \mathbf{L} \mathbf{N}_R$, where \mathbf{N}_R has full row rank, and Eq. (42) is replaced by

$$\bar{\mathbf{C}}^s = -\mathbf{L}(\mathbf{N}_R \bar{\mathbf{E}}_c \mathbf{L})^{-1} \mathbf{N}_R. \quad (44)$$

The response matrices with respect to system parameters p_m read

$$\bar{\mathbf{R}}_p^s = \frac{\partial \mathbf{s}}{\partial \mathbf{p}} = \bar{\mathbf{C}}^s \bar{\mathbf{E}}_p, \quad \bar{\mathbf{R}}_p^j = \frac{\partial \mathbf{j}}{\partial \mathbf{p}} = \bar{\mathbf{C}}^j \bar{\mathbf{E}}_p. \quad (45)$$

Scaled control and response matrices, e.g., $R_u^{s_i} = \partial \ln s_i / \partial \ln u$, are defined and computed in analogy to the scaled elasticities. Since the enzyme concentrations are prefactors in the rate laws, scaled response coefficients and scaled control coefficients are identical. If our perturbation parameters are external metabolite concentrations, this is not the case.

Second-order response coefficients For general perturbation parameters u_p and u_q (i.e., not necessarily enzyme levels), we can write the unscaled second-order response tensors [36] as

$$\bar{R}_{u_p u_q}^{s_i} = \sum_k \bar{C}_{v_l}^{s_i} \Gamma_{u_p u_q}^{v_l}, \quad \bar{R}_{u_p u_q}^{j_l} = \sum_k \bar{C}_{v_l}^{j_l} \Gamma_{u_p u_q}^{v_l} \quad (46)$$

with a tensor Γ defined as

$$\Gamma_{u_p u_q}^{v_l} = \sum_{ij} \bar{E}_{c_i c_j}^{v_l} \bar{R}_{u_p}^{s_i} \bar{R}_{u_q}^{s_j} + \sum_j \bar{E}_{c_j u_p}^{v_l} \bar{R}_{u_q}^{s_j} + \sum_i \bar{E}_{c_i u_q}^{v_l} \bar{R}_{u_p}^{s_i} + \bar{E}_{u_p u_q}^{v_l}. \quad (47)$$

For enzyme levels with their specific restrictions (only one enzyme per reaction, level appears as a linear prefactor in rate law), this translates into the unscaled response coefficients (see Eq. (68))

$$\bar{R}_{u_l u_j}^y = \bar{C}_{v_k}^y \left[\bar{E}_{c_q c_r}^{v_k} \bar{C}_{v_l}^{s_q} \bar{C}_{v_j}^{s_r} v_l v_j + \delta_{kj} \bar{E}_{c_q}^{v_k} \bar{C}_{v_l}^{s_q} v_l + \delta_{kl} \bar{E}_{c_r}^{v_k} \bar{C}_{v_j}^{s_r} v_j \right] \frac{1}{u_l u_j}. \quad (48)$$

The scaled second-order response coefficients between an output y and two enzyme levels u_l and u_j read (see Eq. (69))

$$R_{u_l u_j}^y = \sum_{kqr} (C_{v_k}^y E_{c_q c_r}^{v_k} C_{v_l}^{s_q} C_{v_j}^{s_r}) + \sum_q (C_{v_j}^y E_{c_q}^{v_j} C_{v_l}^{s_q}) + \sum_r (C_{v_l}^y E_{c_r}^{v_l} C_{v_j}^{s_r}) - (C_{v_l}^y C_{v_j}^y) + (\delta_{lj} C_{v_l}^y) \quad (49)$$

The second-order response coefficients can refer to second-order effects of one enzyme (indices $l = j$) or actual enzyme pairs (indices $l \neq j$). For enzyme pairs, δ_{lj} vanishes and we can set $E_{c_i}^{v_l} C_{v_j}^{s_i} = C_{v_j}^{j_l}$ (see Eq. 42). By rewriting the second-order elasticities $E_{c_q c_r}^{v_k}$ as in Eq. 28 and rearranging Eq. (49), we obtain

$$R_{u_l u_j}^y = C_{v_l}^y C_{v_j}^{j_l} + C_{v_j}^y C_{v_l}^{j_j} - C_{v_l}^y C_{v_j}^y + \sum_{kqr} C_{v_k}^y \vartheta_{qr}^k C_{v_l}^{j_k} C_{v_j}^{j_k}. \quad (50)$$

For nonregulated mass-action rate laws close to equilibrium, the term ϑ_{qr}^k can be approximated by -1.

1.3 Spectral power densities and temporal variation caused by chemical noise

To quantify the metabolic fluctuations caused by chemical noise, we start from the chemical Langevin equation for particle numbers x_i and propensities a_l^\pm . The propensities denote the probabilities per time (in s^{-1}) for events of reaction l in forward (+) or reverse (-) direction.

$$\frac{d\mathbf{x}}{dt} = \mathbf{N}^{\text{int}} [\mathbf{a}^+ - \mathbf{a}^-] + \mathbf{N}^{\text{int}} \left[\text{Dg} \left(\sqrt{\mathbf{a}^+} \right) \boldsymbol{\xi}^+ - \text{Dg} \left(\sqrt{\mathbf{a}^-} \right) \boldsymbol{\xi}^- \right] \quad (51)$$

where $\boldsymbol{\xi}^+$ and $\boldsymbol{\xi}^-$ are vectors of standard Gaussian white noise⁴ (in units of $s^{-1/2}$). If we consider a volume Ω , molecule numbers and propensities can be expressed by concentrations and reaction rates as

$$x_i = N_A \Omega c_i, \quad a_l^\pm = N_A v_l^\pm \quad (52)$$

with Avogadro's constant $N_A \approx 6 \cdot 10^{23} \text{ mol}^{-1}$. We can rewrite the chemical Langevin equation as

$$\frac{d\mathbf{c}}{dt} = \mathbf{N}^{\text{int}} \frac{1}{\Omega} \mathbf{v} + \mathbf{N}^{\text{int}} \frac{1}{\Omega} \left[\text{Dg} \left(\sqrt{\frac{\mathbf{v}^+}{N_A}} \right) \boldsymbol{\xi}^+ - \text{Dg} \left(\sqrt{\frac{\mathbf{v}^-}{N_A}} \right) \boldsymbol{\xi}^- \right]. \quad (53)$$

⁴The white noise appears in the formula as the formal derivative of a standard Wiener process. It has the covariance function $\text{cov}_\xi(\tau) = \langle \xi(t) \xi(t + \tau) \rangle_t = \delta(\tau)$ (in s^{-1}) and a spectral power density $S_\xi(\omega) = \frac{1}{2\pi}$ (unitless). Note that we use the following convention for Fourier transforms: $x(t) = \int_{-\infty}^{\infty} \bar{x}(\omega) e^{i\omega t} d\omega$ and $\bar{x}(\omega) = \frac{1}{2\pi} \int_{-\infty}^{\infty} x(t) e^{-i\omega t} dt$.

For deviations Δc_i from a stationary state, and setting $\boldsymbol{\xi} = \begin{pmatrix} \xi^+ \\ \xi^- \end{pmatrix}$, we can approximate it by

$$\frac{d\Delta \mathbf{c}}{dt} = \mathbf{N}^{\text{int}} \hat{E}_c^v \Delta \mathbf{c} + \mathbf{N}^{\text{int}} \hat{E}_\xi^v \boldsymbol{\xi} \quad (54)$$

with elasticity matrices

$$\hat{E}_c^v = \frac{1}{\Omega} \frac{\partial \mathbf{v}}{\partial \mathbf{c}}, \quad \hat{E}_\xi^v = \frac{1}{\Omega \sqrt{N_A}} \left(\text{Dg} \left(\sqrt{\mathbf{v}^+} \right), -\text{Dg} \left(\sqrt{\mathbf{v}^-} \right) \right) \quad (55)$$

in units of s^{-1} and $\text{mM s}^{-1/2}$, respectively. Treating Eq. (54) as a standard linear model with a vector $\boldsymbol{\xi}$ of perturbation parameters, we can compute the frequency-response matrices (see [39])

$$\begin{aligned} R_\xi^s(\omega) &= -\mathbf{L} (\mathbf{N}_R \hat{E}_c^v \mathbf{L} - i \omega \mathbf{I})^{-1} \mathbf{N}_R \hat{E}_\xi^v \\ R_\xi^j(\omega) &= \Omega \left[\hat{E}_\xi^v + \hat{E}_c^v R_\xi^s(\omega) \right] \end{aligned} \quad (56)$$

in units of $\text{mM s}^{1/2}$ and $\text{mol s}^{-1/2}$, respectively. The spectral power density of the concentration fluctuations is then given by

$$S_c(\omega) = R_\xi^s(\omega) S_c(\omega) R_\xi^{s\dagger}(\omega) = \frac{1}{2\pi} R_\xi^s(\omega) R_\xi^{s\dagger}(\omega) \quad (57)$$

(in $\text{mM}^2 \text{s}$) and accordingly for flux fluctuations (in $\text{mol}^2 \text{s}^{-1}$). Next, we can consider fluctuations on a certain time scale σ (unit s). Instead of the fluctuating concentration curve, we consider a smoothed version of it that we obtain by convolving it with a (normalised) Gaussian function of width σ . This function will have the spectral power density

$$S_c^{(\sigma)}(\omega) = (e^{-\frac{1}{2}\omega^2 \sigma^2})^2 S_c(\omega) \quad (58)$$

where the function in brackets is the Fourier transform of our Gaussian function. The covariance function of the smoothed curve is given by the reverse Fourier transform of the spectral power density

$$\text{cov}_c^{(\sigma)}(\tau) = \int_{-\infty}^{\infty} S_c^{(\sigma)}(\omega) e^{i\omega \tau} d\omega, \quad (59)$$

and the variance (the covariance function for time shift $\tau = 0$) is therefore

$$\text{cov}_c^{(\sigma)} = \int_{-\infty}^{\infty} S_c^{(\sigma)}(\omega) d\omega = \frac{1}{2\pi} \int_{-\infty}^{\infty} e^{-\omega^2 \sigma^2} R_\xi^s(\omega) R_\xi^{s\dagger}(\omega) d\omega \quad (60)$$

An analogous formula holds for fluctuations of fluxes.

I.4 Synergy measure Eq. (15)

The effect of a double enzyme perturbation on an output variable y can be formally split into the effects of the single inhibitions plus a rest term $\bar{\eta}_{ab}$, which we call the synergy effect:

$$\Delta y^{ab} = \Delta y_a + \Delta y_b + \bar{\eta}_{ab}. \quad (61)$$

The synergy effect $\bar{\eta}_{ab}$ is thus simply defined as the difference $\bar{\eta}_{ab} = \Delta y^{ab} - \Delta y_a - \Delta y_b$. For small perturbations, we can approximate it using the metabolic response coefficients. A second-order Taylor expansion for a vector $\Delta \mathbf{u}$ of enzyme changes, yields

$$y(\mathbf{u} + \Delta \mathbf{u}) \approx y(\mathbf{u}) + \bar{\mathbf{R}}_{\mathbf{u}}^y \Delta \mathbf{u} + \frac{1}{2} \Delta \mathbf{u}^\top \bar{\mathbf{R}}_{\mathbf{u}\mathbf{u}}^y \Delta \mathbf{u}. \quad (62)$$

If two enzyme concentrations u_a and u_b are decreased by Δu_a and Δu_b , respectively, the output will change by

$$\Delta y^{ab} \approx -\bar{R}_{u_a}^y \Delta u_a - \bar{R}_{u_b}^y \Delta u_b + \frac{1}{2} \bar{R}_{u_a u_a}^y \Delta u_a^2 + \bar{R}_{u_a u_b}^y \Delta u_a \Delta u_b + \frac{1}{2} \bar{R}_{u_b u_b}^y \Delta u_b^2. \quad (63)$$

The single perturbations yield

$$\begin{aligned} \Delta y_a &\approx -\bar{R}_{u_a}^y \Delta u_a + \frac{1}{2} \bar{R}_{u_a u_a}^y \Delta u_a^2 \\ \Delta y_b &\approx -\bar{R}_{u_b}^y \Delta u_b + \frac{1}{2} \bar{R}_{u_b u_b}^y \Delta u_b^2. \end{aligned} \quad (64)$$

With the second-order approximation Eqs (62) and (63), the synergy is given by the second-order unscaled response coefficient $\bar{R}_{u_a u_b}^y$ multiplied by the perturbations:

$$\bar{\eta}_{ab} \approx \Delta y^{ab} - \Delta y_a - \Delta y_b \approx \bar{R}_{u_a u_b}^y \Delta u_a \Delta u_b. \quad (65)$$

If all quantities (enzyme levels and output variable) are measured on logarithmic scale, it is natural to consider the splitting

$$\Delta \log y^{ab} = \Delta \log y_a + \Delta \log y_b + \eta_{ab}. \quad (66)$$

It corresponds to a ‘‘null hypothesis’’ of multiplicative effects, contains the scaled synergy η_{ab} , and in the corresponding formulae the scaled response coefficients are used.

I.5 Second-order response coefficients Eq. (49)

Response coefficients for stationary concentrations and fluxes The unscaled second-order response coefficients between general parameters u_l and u_j and state variables y (stationary concentrations and fluxes) read (as in Eq. (46) and using Einstein's sum convention):

$$\bar{R}_{u_l u_j}^y = \bar{C}_{v_k}^y \Gamma_{u_l u_j}^{v_k} = \bar{C}_{v_k}^y \left[\bar{E}_{c_q c_r}^{v_k} \bar{R}_{u_l}^{s_q} \bar{R}_{u_j}^{s_r} + \bar{E}_{c_q u_j}^{v_k} \bar{R}_{u_l}^{s_q} + \bar{E}_{u_l c_r}^{v_k} \bar{R}_{u_j}^{s_r} + \bar{E}_{u_l u_j}^{v_k} \right]. \quad (67)$$

If the perturbation parameters u_l and u_j are enzyme levels, we can write the elasticities as $\bar{E}_{c_q u_j}^{v_k} = \delta_{kj} \frac{1}{u_j} \bar{E}_{c_q}^{v_k}$, $\bar{E}_{c_r u_l}^{v_k} = \delta_{kl} \frac{1}{u_l} \bar{E}_{c_r}^{v_k}$, $\bar{E}_{u_l u_j}^{v_k} = 0$, and set $\bar{R}_{u_l}^{s_i} = \bar{C}_{v_l}^{s_i} \frac{v_l}{u_l}$. By inserting this into Eq. (67), we obtain

$$\begin{aligned} \bar{R}_{u_l u_j}^y &= \bar{C}_{v_k}^y \left[\bar{E}_{c_q c_r}^{v_k} \bar{R}_{u_l}^{s_q} \bar{R}_{u_j}^{s_r} + \delta_{kj} \frac{1}{u_j} \bar{E}_{c_q}^{v_k} \bar{R}_{u_l}^{s_q} + \delta_{kl} \frac{1}{u_l} \bar{E}_{c_r}^{v_k} \bar{R}_{u_j}^{s_r} \right] \\ &= \bar{C}_{v_k}^y \left[\bar{E}_{c_q c_r}^{v_k} \bar{C}_{v_l}^{s_q} \bar{C}_{v_j}^{s_r} v_l v_j + \delta_{kj} \bar{E}_{c_q}^{v_k} \bar{C}_{v_l}^{s_q} v_l + \delta_{kl} \bar{E}_{c_r}^{v_k} \bar{C}_{v_j}^{s_r} v_j \right] \frac{1}{u_l u_j}, \end{aligned} \quad (68)$$

which is equivalent to the formula given in [36]. The scaled second-order response coefficients read, in analogy to Eq. (18),

$$\begin{aligned} R_{u_l u_j}^y &= \frac{u_l u_j}{y} \bar{R}_{u_l u_j}^y - \frac{u_l u_j}{y^2} \bar{R}_{u_l}^y \bar{R}_{u_j}^y + \delta_{lj} \frac{u_l}{y} \bar{R}_{u_l}^y \\ &= \frac{1}{y} \bar{C}_{v_k}^y \left[\bar{E}_{c_q c_r}^{v_k} \bar{C}_{v_l}^{s_q} \bar{C}_{v_j}^{s_r} v_l v_j + \delta_{kj} \bar{E}_{c_q}^{v_k} \bar{C}_{v_l}^{s_q} v_l + \delta_{kl} \bar{E}_{c_r}^{v_k} \bar{C}_{v_j}^{s_r} v_j \right] - \frac{1}{y^2} \bar{C}_{v_l}^y \bar{C}_{v_j}^y v_l v_j + \delta_{lj} \frac{1}{y} \bar{C}_{v_l}^y \end{aligned} \quad (69)$$

They can be written – again with sum symbols – as

$$R_{u_l u_j}^y = \sum_{krq} (C_{v_k}^y E_{c_q c_r}^{v_k} C_{v_l}^{s_q} C_{v_j}^{s_r}) + \sum_q (C_{v_j}^y E_{c_q}^{v_j} C_{v_l}^{s_q}) + \sum_r (C_{v_l}^y E_{c_r}^{v_l} C_{v_j}^{s_r}) - (C_{v_l}^y C_{v_j}^y) + (\delta_{lj} C_{v_l}^y) \quad (70)$$

Response coefficients for general state variables The previous formulae hold if the output y is a stationary concentration s_i or a flux j_l . How can we generalise them to other output variable $z(\mathbf{c}, \mathbf{v})$, which are functions of the state variables y_p , i.e. metabolite levels and fluxes)? The unscaled derivatives are called \bar{z}_{y_p} and $\bar{z}_{y_p y_q}$. We shall first compute the unscaled, and then the scaled response coefficients of z . The unscaled response coefficients read (with sum convention)

$$\bar{R}_{u_l}^z = \frac{\partial z}{\partial u_l} = \frac{\partial z}{\partial y_p} \frac{\partial y_p}{\partial u_l} = \bar{z}_{y_p} \bar{R}_{u_l}^{y_p}. \quad (71)$$

For the next step, we introduce the the scaled derivatives $\hat{z}_{y_p} = \frac{\partial \ln y}{\partial \ln |y_p|}$ and $\hat{z}_{y_p y_q} = \frac{\partial^2 \ln y}{\partial \ln |y_p| \partial \ln |y_q|}$ and, with their help, rewrite the unscaled derivatives as

$$\begin{aligned} \bar{z}_{y_p} &= \frac{z}{y_p} \hat{z}_{y_p} \\ \bar{z}_{y_p y_q} &= \frac{z}{y_p y_q} \left[\hat{z}_{y_p y_q} + \hat{z}_{y_p} \hat{z}_{y_q} - \delta_{pq} \hat{z}_{y_p} \right]. \end{aligned} \quad (72)$$

The second-order unscaled response coefficients for the output z read

$$\begin{aligned} \bar{R}_{u_l u_j}^z &= \frac{\partial^2 z}{\partial u_l \partial u_j} = \frac{\partial}{\partial u_j} \bar{R}_{u_l}^z = \frac{\partial}{\partial u_j} \left[\frac{\partial z}{\partial y_p} \bar{R}_{u_l}^{y_p} \right] = \left[\frac{\partial}{\partial u_j} \frac{\partial z}{\partial y_p} \right] \bar{R}_{u_l}^{y_p} + \bar{z}_{y_p} \bar{R}_{u_l u_j}^{y_p} \\ &= \left[\frac{\partial^2 z}{\partial y_p y_q} \frac{\partial y_q}{\partial u_j} \right] \bar{R}_{u_l}^{y_p} + \bar{z}_{y_p} \bar{R}_{u_l u_j}^{y_p} = \left[\bar{z}_{y_p y_q} \bar{R}_{u_j}^{y_p} \right] \bar{R}_{u_l}^{y_p} + \bar{z}_{y_p} \bar{R}_{u_l u_j}^{y_p} \\ &= \bar{z}_{y_p y_q} \bar{R}_{u_l}^{y_p} \bar{R}_{u_j}^{y_q} + \bar{z}_{y_p} \bar{R}_{u_l u_j}^{y_p}. \end{aligned} \quad (73)$$

Let us now consider the scaled response coefficients. The first-order scaled response coefficients read

$$R_{u_l}^z = \frac{u_l}{z} \bar{R}_{u_l}^z = \frac{u_l}{z} \bar{z}_{y_p} \bar{R}_{u_l}^{y_p} = \hat{z}_{y_p} R_{u_l}^{y_p}. \quad (74)$$

The second-order scaled response coefficients read (compare Eq. 71)

$$\begin{aligned} R_{u_l u_j}^z &= \frac{u_l u_j}{z} \bar{R}_{u_l u_j}^z - \frac{u_l u_j}{z^2} \bar{R}_{u_l}^z \bar{R}_{u_j}^z + \delta_{lj} \frac{u_l}{z} \bar{R}_{u_l}^z \\ &= \frac{u_l u_j}{z} \left[\bar{z}_{y_p y_q} \bar{R}_{u_l}^{y_p} \bar{R}_{u_j}^{y_q} + \bar{z}_{y_p} \bar{R}_{u_l u_j}^{y_p} \right] - R_{u_l}^z R_{u_j}^z + \delta_{lj} R_{u_l}^z \\ &= \left[\hat{z}_{y_p y_q} + \hat{z}_{y_p} \hat{z}_{y_q} - \delta_{pq} \hat{z}_{y_p} \right] R_{u_l}^{y_p} R_{u_j}^{y_q} + \hat{z}_{y_p} R_{u_l u_j}^{y_p} - \hat{z}_{y_p} R_{u_l}^{y_p} \hat{z}_{y_q} R_{u_j}^{y_q} + \delta_{lj} \hat{z}_{y_p} R_{u_l}^{y_p} \\ &= \hat{z}_{y_p y_q} R_{u_l}^{y_p} R_{u_j}^{y_q} + \hat{z}_{y_p} R_{u_l u_j}^{y_p} - \delta_{pq} \hat{z}_{y_p} R_{u_l}^{y_p} R_{u_j}^{y_q} + \delta_{lj} \hat{z}_{y_p} R_{u_l}^{y_p} \end{aligned} \quad (75)$$

For functions $z(\mathbf{c}, \mathbf{v})$ that are linear if all quantities are given on logarithmic scale (i.e., multiplicative in fluxes and concentrations), the first term vanishes.